Harmonizing Energies: The Interplay Between a Nonplanar SalEn-Type Molecule and a TEMPO Moiety in a New Hybrid Energy-Storing Redox-Conducting Polymer

Anatoliy A. Vereshchagin, Alexey I. Volkov, Julia V. Novoselova, Naitik A. Panjwani, Andrei N. Yankin, Vladimir V. Sizov, Daniil A. Lukyanov, Jan Behrends and Oleg V. Levin*

A. A. Vereshchagin, A. I. Volkov, J. V. Novoselova, V. V. Sizov, D. A. Lukyanov, O.V. Levin
Saint Petersburg State University 7/9 Universitetskaya nab., St. Petersburg, 199034, Russian Federation
E-mail: o.levin@spbu.ru

A. A. Vereshchagin, N. A. Panjwani, J. Behrends
Berlin Joint EPR Lab, Fachbereich Physik Freie Universität Berlin 14195 Berlin, Germany

A. N. Yankin
ITMO University Kronverksky Pr. 49, bldg. A, St. Petersburg, 197101, Russian Federation

Keywords: organic radical batteries, redox conducting polymers, charge transfer, TEMPO, *operando* spectroelectrochemistry

Redox-conducting polymers based on SalEn-type complexes have attracted considerable attention due to their potential applications in electrochemical devices. However, their charge transfer mechanisms, physical, and electrochemical properties remain unclear, hindering their rational design and optimization. This study aims to address this issue by investigating the properties of two novel SalEn-type complexes, poly[N,N'-bis(salicylidene)propylene-2-(hydroxy)diaminonickel(II)] (NiMeSalP(OH)En) and its TEMPO-containing analog, MTS. Introducing TEMPO into the bridge moiety enhanced the specific capacity of the pMTS polymeric material to 71 mA h g^{-1} even at a high rate of 20C, attributed to TEMPO's charge storage capabilities. To elucidate the charge transfer mechanism in the polymer, *operando* UV-Vis spectroelectrochemical analysis, electrochemical impedance spectroscopy, and *ex situ* electron paramagnetic resonance were employed. Replacement the ethylenediimino- bridge with a 1,3-propylenediimino- bridge induced significant changes in the material's

1

morphology, electrochemical and spectral properties. At nearly the same potential, polaron and bipolaron particles emerged, suggesting intriguing features at the overlap point of the electroactivity potentials ranges of polaron-bipolaron and TEMPO, such as a disruption in the connection between TEMPO and the conjugation chain or intramolecular charge transfer. These findings provide valuable insights into the electrochemical characteristics of redox-conducting polymers containing organic radicals, with implications for organic batteries and supercapacitors.

1. Introduction

In recent years, there has been a growing interest in redox polymers due to their versatile properties and synthetic approaches.[1] Among the promising applications of redox polymer materials, their role in energy-related fields stands out.[2,3] Meeting the ever-increasing global demand for electrical energy storage represents one of the greatest contemporary challenges. While lithium-ion technology, introduced in the 1990s, currently reigns as the most advanced battery system,[4] specific applications such as the Internet of Things, flexible devices, smart clothing, wearable electronics, and more have distinct requirements. These include fast charging, outstanding cycle life, mechanical flexibility, safety, absence of toxic metals, facile manufacturing, and processing.[2,5] In many respects, organic polymer electrode materials meet these demands. Recent trends in the field of polymer-based electrode materials have led to a proliferation of studies focused on organic nitroxyl radical-bearing polymers.[6–9] Specifically, a stable nitroxyl radical 2,2,6,6-tetramethylpiperidinyl-N-oxyl (TEMPO) has gained prominence since its original report in 2002.[10] In this context, 2,2,6,6-tetramethylpiperidinyloxy methacrylate (PTMA) was employed as cathode active material in subsequent reports.[11–14] The advantages of this radical polymer and its derivatives include great reversibility, high voltage vs. Li anode (3.5 V), decent theoretical specific capacity of 111 mA h g^{-1}, and high-rate capability with reported values of up to 1500C.[14–16] Aside from polymethacrylate, subsequent studies have explored multiple various other polymers[17] — ranging from aliphatic[18,19] to conjugated[20–23] — as TEMPO-bearing polymer backbones. The need for conjugated (or conducting) backbones arises from the low electrical conductivity of not-conjugated compounds. Insufficient charge transport within the material requires the addition of conductive components (e.g., carbon black) to the electrodes, thereby decreasing the total specific capacity of the electrodes. Radical polymers with conductive backbones are

designed to eliminate this limitation, as organic radicals and conjugated polymers synergistically enhance each other's properties. The former stores charge via redox transformations, while the latter provides electronic conductivity through a system of conjugated π-bonds, serving as an electric charge sink.[21] However, careful selection of a backbone, linker, and the radical is essential, as introduction of side chain may affect the charge mobility, increase electric resistance, and thus negatively affect the specific power.[23] Another benefit of conducting polymers is that they can be produced by electrochemical polymerization, a viable approach for fabricating flexible thin-film devices. Most studies on organic radical batteries have primarily involved polymer backbones with negligible inherent capacity. A promising route for further enhancement of organic electrode materials involves linking the TEMPO pendant group to a conducting polymer with inherent redox capacity. In this configuration both components would contribute to conductivity — close-range electron hopping between pendant group radicals and long-range electron transfer via conjugated π-system of the conducting polymer. Additionally, both components contribute to the material charge storing capabilities. One such option is nickel-SalEn (N,N'-bis(salicylidene)ethylenediamine) type polymers that have been explored as both conducting agent and binder,[24] as well as standalone electrode for battery application.[25] Recently, we have reported a redox-conducting polymer based on polyNiSalEn conductive backbone with two pendant TEMPO groups per unit (pDiTS), providing a specific capacitance of up to 91.5 mA h g^{-1} and high rate capability.[26] Our investigation of electrochemical cells with spectroelectrochemical electron paramagnetic resonance (EPR) measurements elucidated the mechanisms of both recharging and degradation of this redox-conductive polymer.[27] In case of pDiTS, an important condition for the effective functioning of hybrid systems[28,29] has been achieved: a complete overlap of the operating potentials of the components. The fortuitously optimal structure presented in the cited work[27] prompts an exploration into whether this optimality is a characteristic feature of the entire class of substances or specific to the presented molecule. Based on the overlapping degree (difference between redox potentials of the component oxidation/reduction processes), hybrid molecules can be divided into optimal, semi-optimal and non-optimal systems. However, despite numerous reports, the relationship between nonredox component properties and redox polymer properties remains unclear. Questions persist regarding the impact of planarity within the conductive backbone on the overall properties or the influence of steric hindrance and molecular packing on the charge transfer efficiency. A slight change in the structure of the conducting polymer may

3

change steric hindrance and affect a variety of the material properties, including specific capacity and ease of charge transfer.[23,30,31] This paper proposes a novel redox-conducting polymer based on non-planar Ni(SalEn) type fragments forming a conductive backbone with a single TEMPO pendant per monomer unit. Our study sets out to investigate the outcome of an approach using a non-planar conductive backbone with relatively low steric hindrance. The work focuses on understanding physical, electrochemical and spectral data and related charge transfer processes, intra- and intermolecular interactions, catalytic effects and degradation processes. By employing a set of electrochemical and spectral techniques, we characterize the redox-conducting TEMPO-containing polymer poly[N,N'-bis(salicylidene)propylene-2-(TEMPO)diaminonickel(II)] - NiMeSalP(TEMPO)En (pMTS) and compare its properties to those of its TEMPO-free counterpart poly[N,N'-bis(salicylidene)propylene-2-(hydroxy)diaminonickel(II)] (pNiMeSalP(OH)En). This research will contribute to a deeper understanding of the processes involved in organic radical batteries and promote further investigations in this area.

2. Results and Discussion

2.1. Synthesis and Characterization of the Monomers

The NiMeSalP(OH)En was synthesized using the same procedure described earlier for NiSalP(OH)En.[32] Attaching TEMPO to the monomeric NiMeSalP(OH)En for the MTS formation was performed using the following procedure described in the literature for 2,3-dihydroxybenzaldehyde (**Figure 1**).[26]
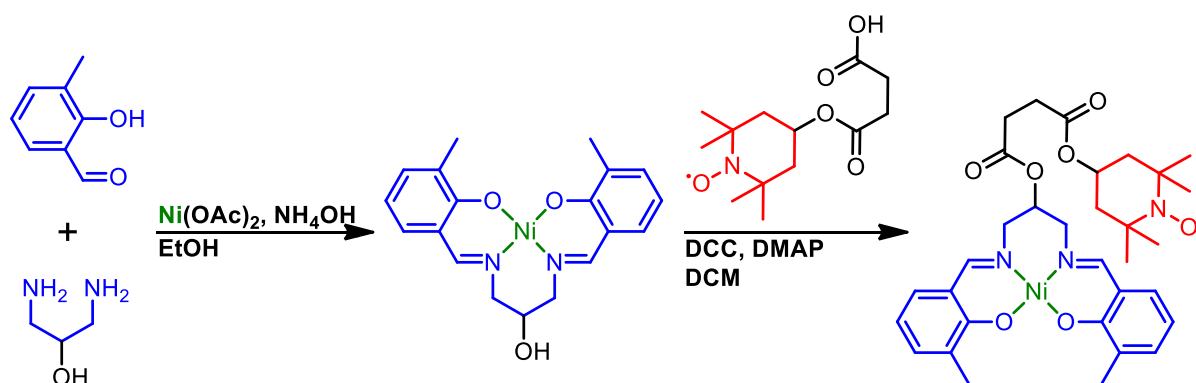
Figure 1. Route of NiMeSalP(OH)En and MTS monomers synthesis (See details in S1.2).

Structures of the NiMeSalP(OH)En and MTS were confirmed by HRMS, FTIR and ^{1}H and ^{13}C NMR (**Figure S2-8, 12**). However, due to the intrinsic transient paramagnetism of the extended-bridge NiMeSalP(OH)En complex,[32] some signals corresponding to the nuclei close to the paramagnetic Ni center are absent in NMR spectra. The observed undesired peaks on ^{1}H NMR of the MTS correspond to the quenching agent, ascorbic acid, and its oxidized form (Figure S7b). The structure of the MTS monomer was additionally confirmed with 2D NMR using correlated spectroscopy (COSY), heteronuclear single quantum coherence (HSQC) and heteronuclear multiple bond correlation (HMBC) techniques (**Figure S9-11**). The attribution of the signals and correlations in the MTS molecule is shown at **Figure 2** and presented with another spectroscopic data in S1.2.2.
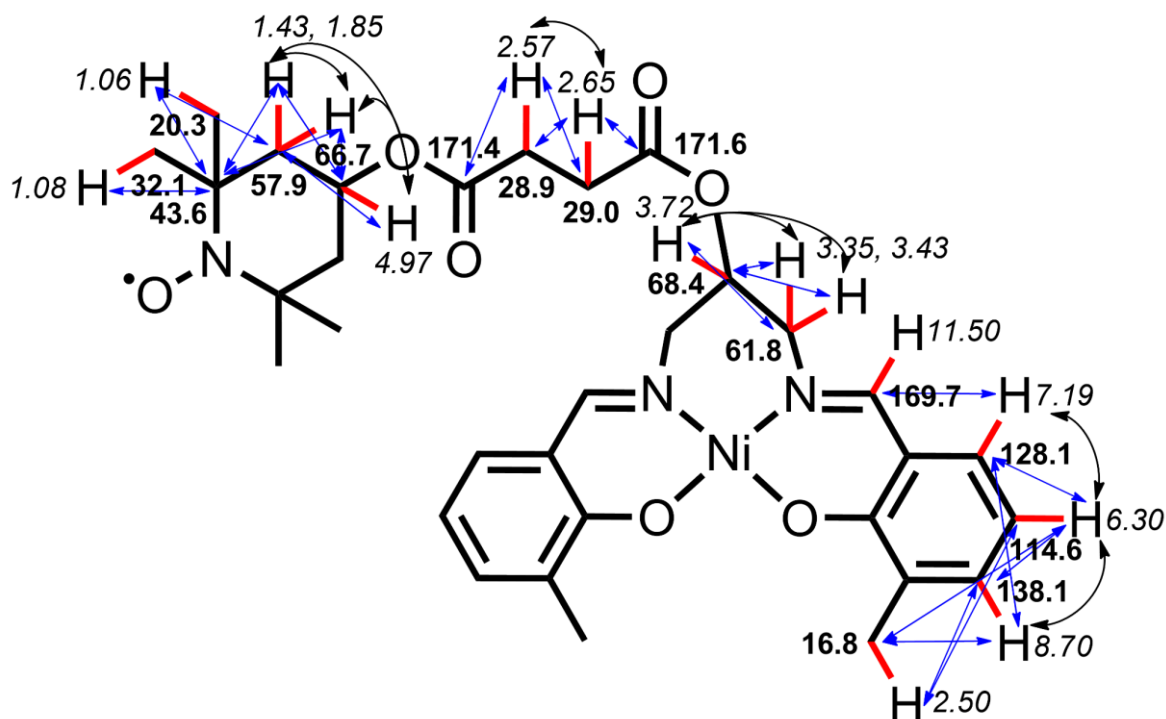

Figure 2. Attribution of the chemical shifts for MTS based on 2D NMR using COSY, HSQC and HMBC techniques.

Density functional theory (DFT) calculations

According to DFT geometry optimizations (see set up details in S1.3.8 section) for the monomers studied here, which we performed to predict the spatial arrangement of the monomer units in the polymers, the phenyl rings in NiMeSalP(OH)En and MTS are

significantly tilted in opposing directions relative to the near-planar NNOO fragment. In this study, the magnitude of this tilt was evaluated as the angle between the planes of two phenyl rings ($\angle$ Ph/Ph), with both of these planes being determined by three non-adjacent carbon atoms belonging to the corresponding ring. For the optimized structure of the neutral NiMeSalP(OH)En complex, the dihedral angle was found to be equal to 41 degrees, while for MTS it was somewhat smaller, 36 degrees (**Figure 3**).

WILEY-VCH

(a)   (b)
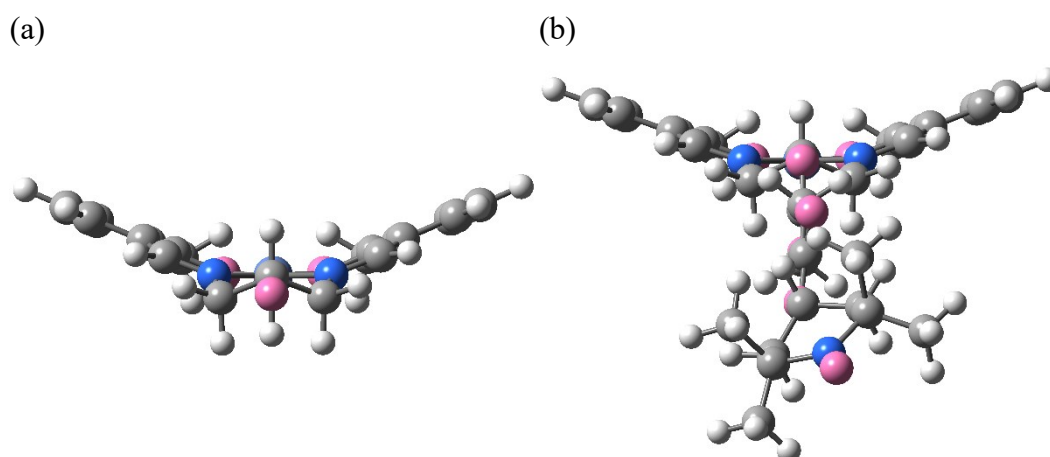
Figure 3. Displaying intramolecular angle for complexes NiMeSalP(OH)En (a) and MTS (b).

This pronounced non-planarity was observed earlier for [NiSalP(OH)En] [32] by X-ray crystal diffraction and is in stark contrast with many well-known quasi-planar nickel complexes with SalEn-type ligands, such as NiSalEn, NiSaltmEn, NiSalPhen and their derivatives, for which the corresponding calculated angles typically do not exceed 4 or 5 degrees (**Table S1**). It is also worth mentioning that a significantly smaller angle of 32 degrees reported in [32] for [NiSalP(OH)En] was obtained using a different approach, namely, as the C–Ni–C plane angle, which is less informative than the criterion used in the present study. For dimers and tetramers, the geometry of MTS units is largely preserved in neutral oligomers, though the Ph/Ph angle between the rings of the same unit does increase in [MTS]$_2$ and [MTS]$_4$, as compared to the monomer complex. Another feature of MTS oligomer, which is typical for other SalEn-type complexes,[33] is the non-coplanar arrangement of neighboring units in the chain. This structural feature was described by the dihedral angle between two phenyl rings belonging to different monomer units and connected by a C–C bond. For NiMeSalP(OH)En and MTS this angle was found to be equal to 40 and 33 degrees, respectively, i.e., close to the value of ca. 35 degrees, which is typical for many neutral SalEn-type nickel complexes, including NiSalEn.[33] Due to the presence of a three-atomic bridging fragment and non-planar complex structure for MTS and NiMeSalP(OH)En, the helix-like structure of the polymers chain is expected.

Continuous wave electron paramagnetic resonance (CW-EPR)

WILEY-VCH

To check the quality of the material after synthesis and the charge state of TEMPO the MTS monomer complex was studied by CW-EPR spectroscopy in a dilute 100 µM concentration sample in toluene at room temperature. In **Figure 4** a three-line structure is observed, which matches that of TEMPOL also measured in a 100 µм toluene sample. The three-line structure arises from the $S=1/2$, $I=1$ system where the nitroxide radical couples to the nitrogen with nuclear spin 1, causing hyperfine splitting that is visible in the CW-EPR spectrum. The three-line structure can be described by isotropic hyperfine coupling, as all anisotropic interactions average out due to molecular tumbling in solution. The EPR spectrum for MTS shows no additional features hence confirming the mono-nitroxide nature of the pendant group. It also suggests the MTS molecular structure does not significantly affect the rotational correlation time (tumbling) of the attached TEMPO group. The quantitative analysis on both MTS and TEMPOL (100 µM samples, 50 µL volume in EPR tube) showed the equal number of spins in each sample (3.1×10^{15} spins or 3.1×10^{18} spins per cm^3) thereby confirming the presence of one TEMPO group per SalEn fragment and the sample's high quality after all synthetic manipulations.
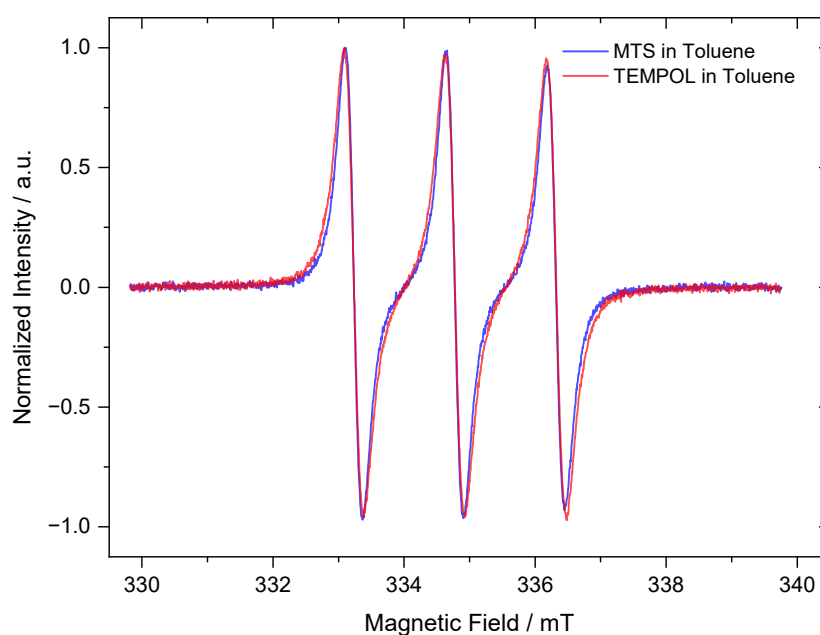

Figure 4. CW-EPR spectra of 100 µM MTS and TEMPOL in toluene solutions at room temperature.

2.2. Electrochemical Polymer Deposition

The polymer films were prepared by electrochemical polymerization, in a manner similar to previously reported materials.[26] As electropolymerization conditions strongly affect the polymer properties, the analysis of the polymerization processes provides insight into the charge transfer within the resulting films. Therefore, we employed the combined cyclic voltammetry / electrochemical quartz crystal microbalance (CV/EQCM) technique on Pt-coated quartz crystals to calibrate the conditions for the efficient synthesis of the films with the highest redox activity for MTS and NiMeSalP(OH)En.

The first cycle of NiMeSalP(OH)En deposition (**Figure 5**a) shows one irreversible anodic peak at 0.65 V which corresponds to the monomer oxidation. In the following cycles, the CV current increases steadily along with the electrode mass (Figure 5a), i.e., polymerization occurs. Two pairs of peaks corresponding to oxidation / reduction (**I**: 0.35 V, **I'**: 0.16 V; **II**: 0.46 V, **II'**: 0.40 V) of the deposited polymer appear in the subsequent cycle. Two consecutive oxidation processes are related to delocalized cation-radicals (polarons) formation followed by their further transformation into dications (bipolarons), which is typical for SalEn-type polymers.[34] The analysis of mass variation during deposition indicates the oxidative coupling of the SalEn fragments in the 0.3–0.7 V potential range producing the pNiMeSalP(OH)En polymer.[35–39] In this case the mass-potential curve of the first cathodic wave has a two-step shape with the first mass increase at 0.4–0.7 V, and the second one at 0.2–0.4 V (cathodic direction). Most likely, the high positive charge of the polymer unit in the thin film due to the bipolaron formation at 0.46 V and emergence of a layer of charge compensating ions solvated by electrolyte molecules can inhibit the free growth of the polymer chain. Subsequent reduction of the bipolaron in the 0.2–0.4 V region leads to an increase of the electrode mass. This mass variation behavior becomes less noticeable with an increase of the polymer loading due to the higher contribution of the mass of the charge compensating ions to the total flux: an increase in mass is observed in the region of oxidation and decreases as the system is reduced.

WILEY-VCH
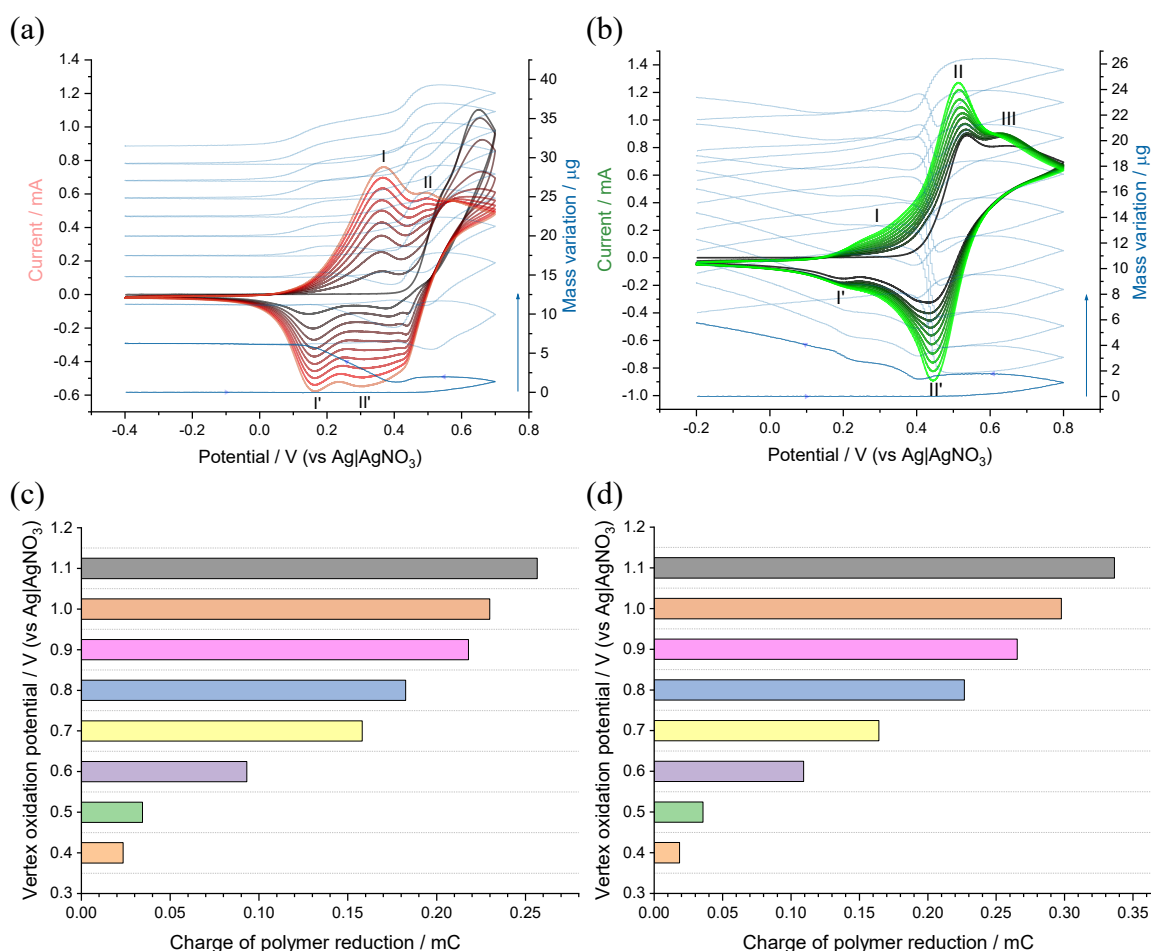
Figure 5. EQCM analysis of the polymerization of NiMeSalP(OH)En (a) and MTS (b) in 1 mM monomer / 0.1 M Et$_4$NBF$_4$ in CH$_3$CN with a scan rate of 50 mV s^{-1}; the analysis of polymerization potentials window during five cycles for NiMeSalP(OH)En (c) and MTS (d) on GC in 1 mM monomer / 0.1 M Et$_4$NBF$_4$ in CH$_3$CN with a scan rate of 50 mV s^{-1}.

Deposition CVs of MTS (Figure 5b) contain a pair of peaks of oxidation (II) at 0.52 V and reduction (II') at 0.45 V, which corresponds to charging and discharging of the nitroxyl fragments. An irreversible anodic peak (**III**) at 0.65 V still corresponds to the monomer oxidation process. Broad signals (**I** and **I'**) are observed in the 0.2–0.5 V range, which is related to the electrochemical activity of the SalEn backbone. Only a part of the charge/discharge signals of the conductive backbone is pronounced, while the second one (**II** at Figure 5a) overlaps with the TEMPO activity window. An additional evidence of that are two steps of mass growth in cathodic wave of the first deposition cycle in the 0.4–0.8 V and 0.2–0.4 V regions, as with NiMeSalP(OH)En (Figure 5a). The notable feature in the EQCM curves for MTS is the mass growth at the electrode occurring even at potentials below the polymer electrical activity (Figure 5b, −0.2–0.2 V). Such behavior contradicts previous

reports on the deposition of a "classic" NiSalEn-type polymer, which polymerizes at the potentials above the oxidation peak of the monomeric NiSalEn.[40] This unique response is most likely because of the charge-carrying TEMPO groups which create a "solvate / coulombic shield" and prevent a typical course of polymerization. This mechanism for another TEMPO-modified SalEn type material — poly di-TEMPOSalEn (pDiTS) bearing two TEMPO groups per monomer unit — was described previously.[26] Obviously, for MTS bearing only one TEMPO group this effect should be less pronounced, yet is still present despite the different arrangement of the TEMPO group. As in the case of pDiTS, for pMTS a sharp drop in mass at anodic wave is observed in subsequent cycles at the TEMPO charging potential at ca. 0.4–0.5 V (where the "shield" "switches on"), which displays the possible ejection of unreacted charged particles from the polymer matrix.

To confirm the selection of the best conditions for polymerization of the monomers, we varied the CV scan boundaries and observed the effect on the process. No redox activity was observed for both monomers while sweeping in −0.4 – 0.4 V range without the polymer formation (**Figure S13**a, b). An extension of the anodic boundary to any potential within the 0.6 – 1.1 V range led to an increase in CV current, which indicates the polymer formation. To avoid the overoxidation of monomers and/or deposited polymer layers, the dependence of polymer reduction charge after the fifth deposition cycle on the range of applied potentials was analyzed. The 0.5 – 0.7 V region for NiMeSalP(OH)En (Figure 5c) corresponds to the largest increase of charge relative to the one at the previous potential range, while further extension of the anodic region of the CV range did not significantly improve the polymerization process. A similar picture is observed for MTS (Figure 5d), but the optimal upper cycling boundary slightly expanded to 0.8 V, which is justified by the redox activity of the TEMPO moieties in the solution. Following these observations, we selected the −0.4 – 0.7 V and −0.4 – 0.8 V regions for NiMeSalP(OH)En and MTS, respectively, as working potentials for the polymerization process.

2.3. Scanning electron microscopy (SEM)

To investigate the polymer film morphology and establish the influence of the monomers' geometry on the films' structure, SEM images were obtained for pNiMeSalP(OH)En and pMTS films deposited on a glassy carbon substrate. The non-modified polymer has globular porous morphology in both reduced (**Figure 6**a) and oxidized (Figure 6b) states with large

gaps and weak interglobular contact. The typical square-planar SalEn-type complexes are characterized by a more homogeneous and even morphology.[25,40–42] A less-connected structure can result in a lower electronic conductivity of the pNiMeSalP(OH)En compared to that of the classic NiSalEn polymer. As seen from **Figure S17**a, b, the polymer film consists of two domains: globular coral-structure formations and thin even polymer film between them. Such polymer layer's structure can be caused by the deviation from a square planar complex structure due to the presence of a triatomic imine bridge bearing an out-of-plane -OH group,[32] which is consistent with the DFT calculations mentioned above. A similar structure was also observed for another complex with a bulky imine fragment which influenced the morphology.[43] pMTS films consist of the same two types of entities in the reduced state (Figure 6c). The formation of coral-like domains for this polymer is less pronounced here (Figure S17c). The smoother layers form in this case, which is likely due to the presence of the sufficiently long succinyl linkers. The same phenomenon occurred in the TEMPO-containing PEDOT based systems,[44] where the lengthening of the linker led to a transition from the globular polymer structure to the smoother film. In the oxidized state (Figure S17d and Figure 6d) there are two different layers of pMTS are formed. The layer closest to the substrate has the same structure as the unmodified polymer. The upper phase is formed by the electrolyte salts (BF_4^-), which was confirmed by EDX analysis (**Figure S18**), and may be due to the strong coupling between charged TEMPO groups and charge compensating BF_4^- ions and/or interaction of the electrolyte ions with oxygen atoms of the succinyl linker. This kind of formation is pretty unique and was not detected for other TEMPO-containing redox-conducting polymers based on the SalEn-type complex.[26]
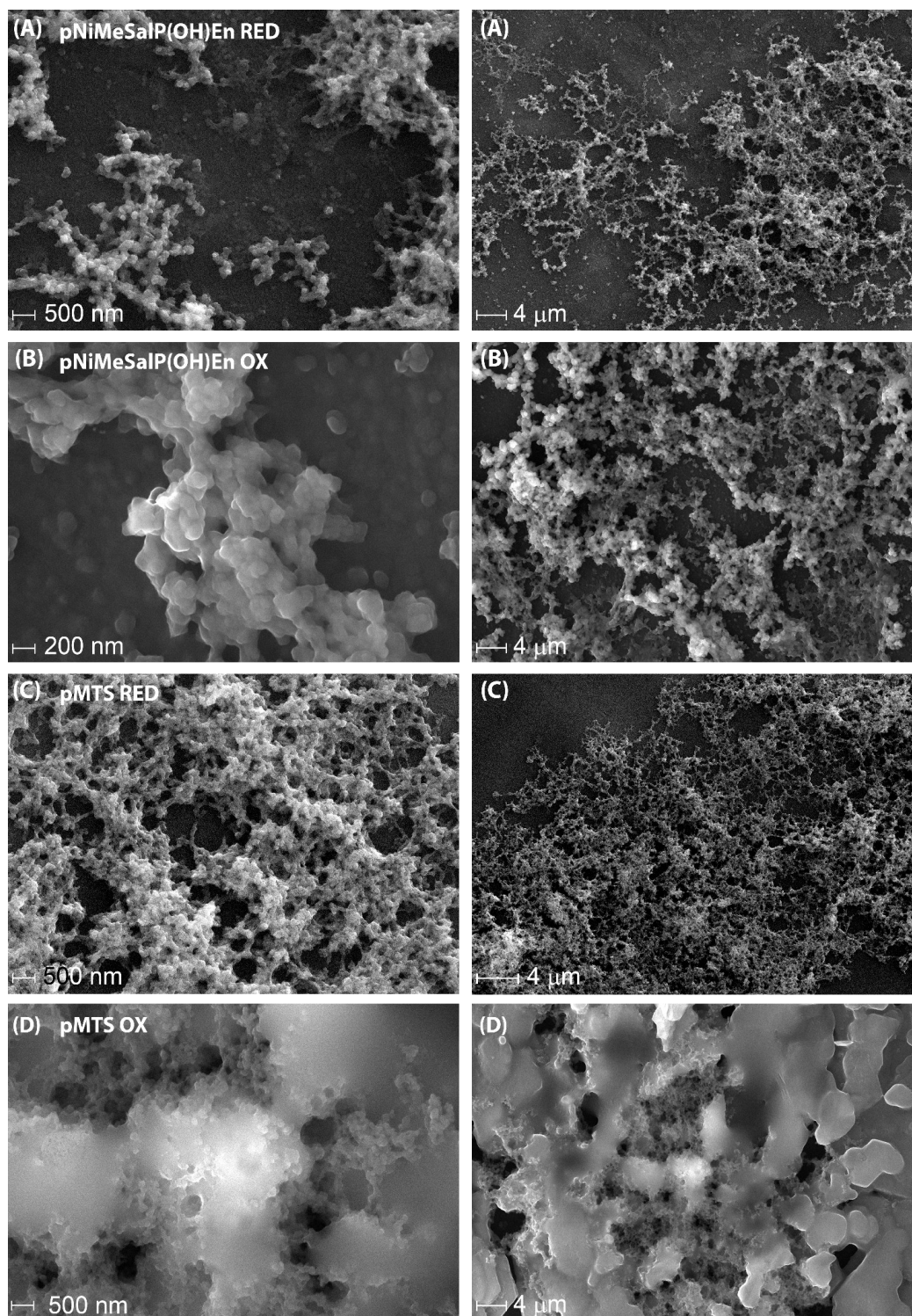
Figure 6. SEM images for thin films of pNiMeSalP(OH)En (a, b in reduced and oxidized states, respectively) and pMTS (c, d in reduced and oxidized states, respectively).

2.4. Electrochemical Performance

To gain insight into the differences in charge and mass transport processes during electrochemical recharging of the polymers, caused by the presence of several redox-active centers in the monomer unit, we initially characterized the deposited films using a combined CV/EQCM technique.

The CV curve of the resulting polymers in a monomer-free 0.1 м Et_4NBF_4 (CH_3CN) electrolyte solution has a multi-peak shape (**Figure 7**a, b) which is typical for conductive polymers.[45–51]

The shape of the CV curves for pNiMeSalP(OH)En (Figure 7a) contains two reduction peaks (ca. 0.17 V and 0.27 V) and one mixed oxidation peak at 0.37 V, containing a shoulder at a more positive potential (0.51 V), which was also noticeable during the synthesis of the polymer. This CV shape is similar to those of pNiSalEn and pNiSalphEn polymers.[41]

In the case of pMTS, two regions — 0.2 – 0.4 V and 0.4 – 0.6 V — can be distinguished (Figure 7b). The first region relates to the electrochemical activity of the SalEn fragment. TEMPO recharge is characterized by one reversible pair of oxidation/reduction peaks at 0.4 – 0.6 V. Compared to the CV of the non-modified complex (Figure 7a), the SalEn-related potential region did not change for pMTS, indicating a lack of the influence of the TEMPO-containing pendent on the π-conjugated system of the complex. This behavior can be associated either with the location of the TEMPO group which is far enough from the SalEn-ligand delocalized π system, partially or completely preventing the charge shielding effect, or with the non-planar structure of the organometallic complex mentioned above.

14

(a)

(b)

(c)

(d)
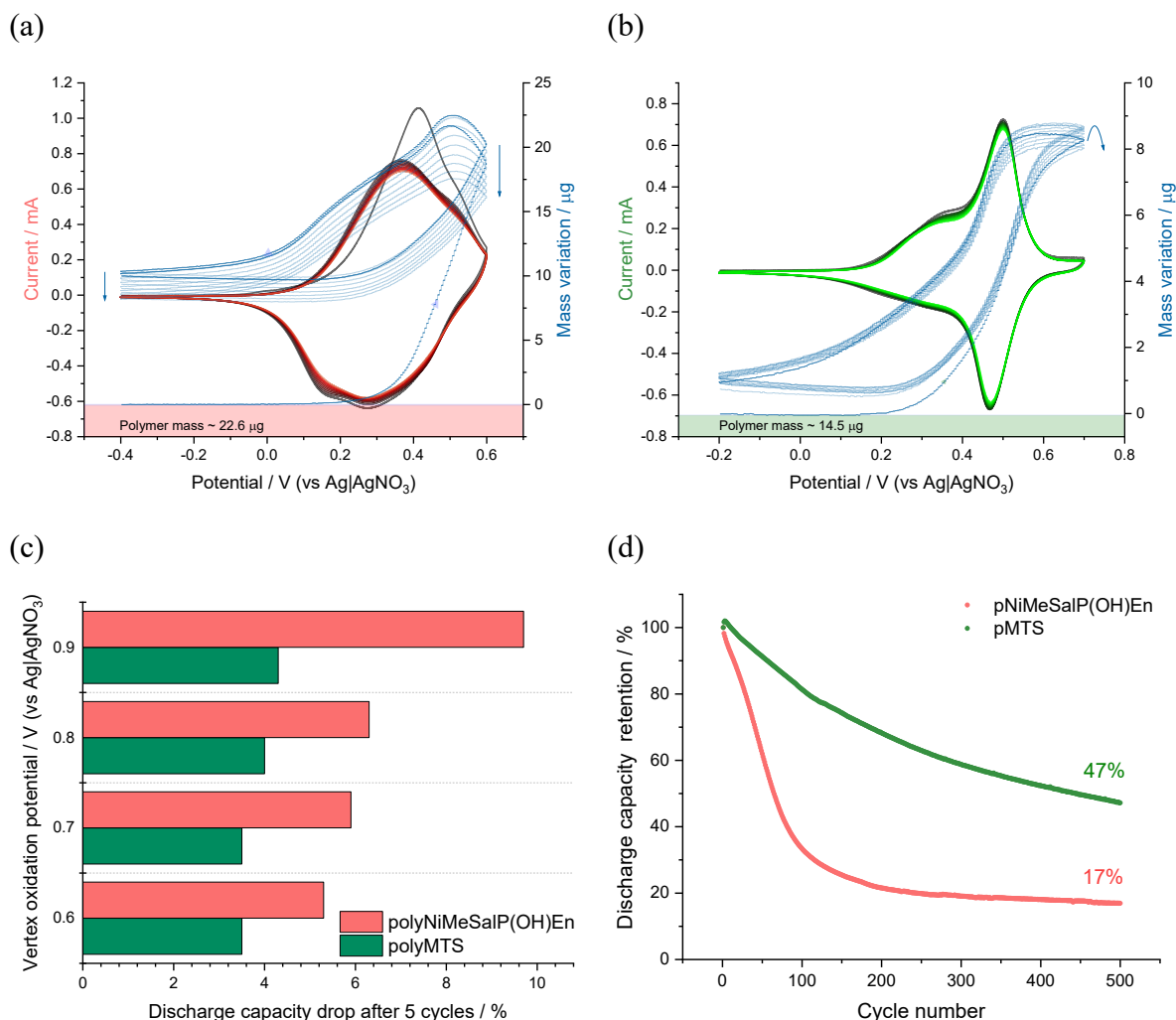
Figure 7. EQCM analysis of the cycling of pNiMeSalP(OH)En (a) and pMTS (b); the analysis of the potential windows within five cycles for studied polymers (c); the analysis of cycling stability for studied polymers (d). All measurements were carried out on GC in monomer-free / 0.1 M Et_4NBF_4 in CH_3CN with a scan rate of 50 mV s^{-1}.

The sharp mass increase in the EQCM curves (Figure 7a, b) in the initial cycles corresponds to the inbound flux of charge-compensating ions accompanied by an irreversible polymer swelling, which added 10 μg and 1 μg to the 23 μg and 14.5 μg mass of the dry film of pNiMeSalP(OH)En and pMTS, respectively. As a result, the film masses regained the values recorded at the last polymerization cycle. The mass difference is thus related to the dry films swelling in the first oxidation cycle in the monomer-free solution. The analysis of the subsequent EQCM curves indicates a gradual dissolution and/ or decreasing insertion extent of anions due to the slow electroactivity loss of both samples, while for pMTS this effect is less pronounced, despite the higher upper vertex potential. The dissolution can be associated

This is a Submitted version before peer review.
Published version available at 10.1002/marc.202400074

WILEY-VCH

with the presence of the -OH group in the structure of the pNiMeSalP(OH)En, as well as with uneven morphology (**Figure 6**).

Stability window and cycle life

A gradual increase of the upper vertex potential from 0.6 V to 0.9 V leads to a noticeable rise in the film degradation rate of pNiMeSalP(OH)En, in contrast to pMTS (Figure 7c). pMTS stabilization with the introduction of TEMPO group into the structure of the complex (Figure 7d) was also observed earlier for pDiTS.[26] These features of pMTS are partially due to the presence of the aforementioned "solvate / coulombic shield", which protects the backbone from interaction with the electrolyte impurities (e.g., water). At the same time, the introduced long succinyl linkers should act as a kind of mobile "cross-linking" system that slows down the dissolution of the polymer. Thus, the introduction of the TEMPO group complex structure increases stability and allows to save 47% of the initial capacity after 500 cycles of charge/discharge, against 17% for the pNiMeSalP(OH)En. Mass flux of charge compensating species in a monomer-free electrolyte, determined from the slopes of the linear regions of mass/charge dependence as reported previously[26,33,35,52] using the Sauerbrey equation,[53] was found to be provided mostly by the BF_4^- ions solvated by acetonitrile molecules (**Figure S19**a, b). Intercalation of these ions compensates the positive charge of the materials, confirming the p-type conductivity nature of the studied polymers at anodic potentials. An increase in the molecular weight of particles in the region of high potentials indicates the possible polymer swelling and the expansion of the film during oxidation which allows additional molecule of solvent and more solvated ions to enter.

Kinetic parameters

For pNiMeSalP(OH)En, as shown during polymerization (Figure 5a), two pairs redox peaks are observed at scan rates up to 50 mV s^{-1} during oxidation, and up to 600 mV s^{-1} during reduction (Figure S19c). The pair of peaks at ca. 0.4 V is not as strongly dependent on the scan rate as the peaks at ca. 0.6 V and ca. 0.2 V, which may be due to the formation of different types of particles at these potentials. As the scan rate increases further, the peaks overlap. For pMTS (Figure S19d), the peak related to the activity of the SalEn backbone (0.3

– 0.4 V) exhibits noticeably higher mobility than the TEMPO/TEMPO$^+$ peak, and they overlap from 600 mV s^{-1} on.

For pNiMeSalP(OH)En, the proportionality between the peak currents and the potential scan rate is observed for scan rates up to 400 mV s^{-1} (Figure S19e), where the current-rate dependence changes from linear to square root behavior, as seen from the bilogarithmic plots of both the anodic and the cathodic peaks current vs scan rate. This indicates a transition from a diffusionless "thin layer model" electrochemical behavior of the film to a semi-infinite diffusion control at higher scan rates.[54] For pMTS, this transition starts at 100 mV s^{-1} (Figure S19f), as the presence of mobile linkers may slow the kinetics of the process. The charged TEMPO groups can also influence the rate of electronic processes in the conductive backbone. The apparent rate constants and the standard electrode potentials of the redox processes in the studied polymers were calculated from the dependence of the peak potential on the logarithm of the potential scan rate using a standard method (Figure S19g, h).[26,55,56] Both polymers show high values of apparent rate constants which indicates fast kinetics of charge transfer. The resulting apparent rate constant, 97.8 s^{-1} and 86.3 s^{-1} (anodic and cathodic processes, respectively) for pNiMeSalP(OH)En indicates faster kinetics relative to other similar materials.[26,56] The open morphology structure of the polymer (coral-like formation instead of a uniform film, **Figure 6**) may support faster mass transport through the material and thus may enhance kinetics. The rate constant of pMTS reached slightly lower value 22.9 s^{-1} for anodic and 17.3 s^{-1} for cathodic processes, likely inhibited by a more complex molecular structure of the polymer. The change in the oxidation/reduction peak positions and their overlapping introduce the main inaccuracies in calculating the rate constants of the reaction and the transfer coefficient (α). Thus, although α for the studied polymers is not equal to 0.5, it is pretty close to this value (0.43–0.57), indicating high reversibility of the oxidation/reduction of the polymers.

Electrochemical behavior at different charge rates

The analysis of the capacity properties of pNiMeSalP(OH)En (**Figure 8**a, red dots) shows the behavior typical for SalEn-type materials. There is an increase in the reversibility of the system and its capacity at lower scan rates. The presence of the second oxidative process (polaron-bipolaron) enhances the specific capacity of the material, which reaches

WILEY-VCH

97 mA h g^{-1}, since the maximum theoretical capacity of a single-electron process is only 70 mA h g^{-1}.

The introduction of TEMPO groups provides an increase in the capacity of the TEMPO-containing material pMTS by ~10–30% (Figure 8. A) at a scan rate of 2–3000 mV s^{-1} and reaches 95 mA h g^{-1}. An increase in capacity was also observed for other TEMPO-containing polymers,[17] including SalEn-type based ones.[26,47] The analysis of the potential difference between the charge/discharge peaks of TEMPO groups in pMTS (**Figure S20**a, b) shows the onset of a small (the growth of the peaks separation by ~1–10 mV) deviation from the equilibrium behavior at speeds below 1 mV s^{-1}, which may be the reason for a diminished capacity contribution, compared to the pNiMeSalP(OH)En, as the scan rate decreases. This behavior can be associated both with the occurrence of side reactions[57] (interaction with residual water in the electrolyte) and with the possible internal charge transfer between the components.[28,29] The deviation of the structure of the complex from the planar one may render the theoretical capacity maximum unattainable.[32]

The electrochemical performance of polymers was also studied in a three-electrode cell by galvanostatic charge-discharge (GCD, Figure 8b) using a symmetric mode for charging and discharging at a current rate of 20C (22 μA cm^{-2} for pNiMeSalP(OH)En and 31 μA cm^{-2} for pMTS). The discharge curves for pMTS exhibit a slightly inclined plateau at ca. 0.53 V, indicative of TEMPO-based redox processes, and sloped regions at 0.25–0.40 V corresponding to the backbone-related redox processes (Figure 8b, green line). The specific capacity of the pMTS films reached 71 mA h g^{-1} and slightly decreased to 66 mA h g^{-1} (1.4% drop per cycle) during five cycles. For pNiMeSalP(OH)En, a GCD curve is more inclined (Figure 8b, red line), which is typical for other SalEn-type complexes [25] and is indicative of a more capacitor-like behavior. The unmodified polymer reached a capacity of 63 mA h g^{-1} and showed a more rapid decrease to 52 mA h g^{-1} (3.5% drop per cycle) during five cycles. The average operating voltage of pMTS is approximately 0.15 V higher than that of pNiMeSalP(OH)En, leading to the increased energy density of a cell with this material.

(a)

(b)
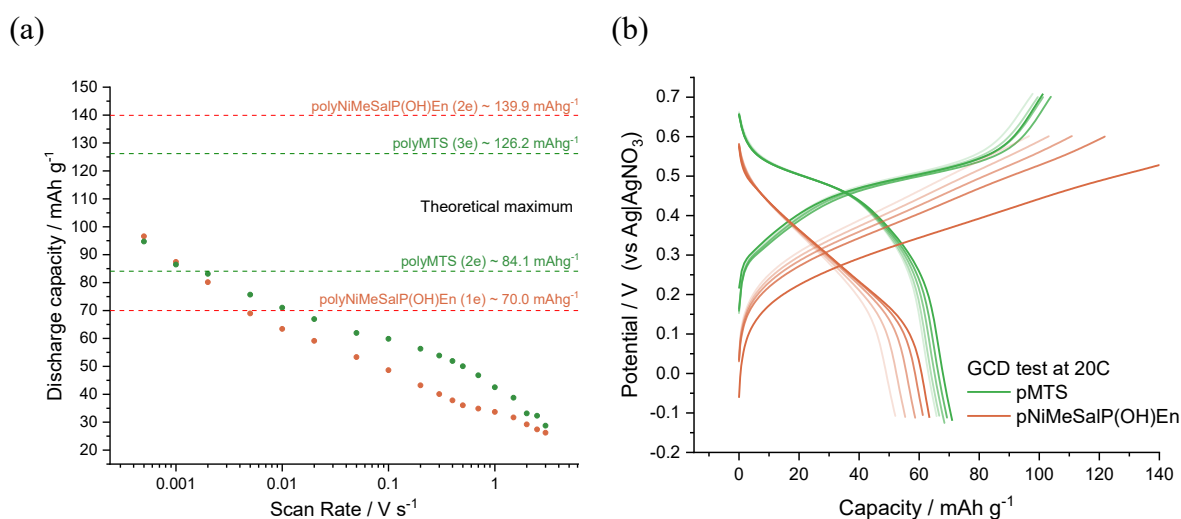
Figure 8. The specific capacity values of pNiMeSalP(OH)En and pMTS measured in 0.1 м Et₄NBF₄ / CH₃CN solution using various potential scan rates (a); GCD curves of pNiMeSalP(OH)En and pMTS at 20C (b).

For both samples, the oxidation process is more pronounced (Coulombic efficiency was 51% and 67% for pNiMeSalP(OH)En and pMTS, respectively). The charge, accumulated during the irreversible oxidation in course of multiple redox cycles is several times exceeding the capacity of the polymer, while the redox activity of the polymer is changing only by few percent. This means that irreversibility cannot be caused by partial degradation of materials. Most likely, prolonged oxidation can lead to the formation of highly active bipolarons that provide catalytic currents. Bipolarons are chemically reduced immediately after the formation through a series of interactions with impurities (e.g., water or Lewis acids), followed by successive oxidation of formed polarons to bipolarons again, forming an electrocatalytic cycle.[57]

2.5. Spectroelectrochemistry and conductivity measurements

To enhance our understanding of charge transfer processes, we employed various spectroscopic methods including EPR and UV-Vis methods. For this purpose, we utilized these spectral methods *in situ* and *operando* to observe and analyze the electrochemical processes in real time. We compared these results with data acquired via pure electrochemical methods, such as conductance measurements and electrochemical impedance spectroscopy.

WILEY-VCH

**2.5.1. Staircase potentio electrochemical impedance spectroscopy (SPEIS) measurements**

The impedance spectra (**Figure 9**) were simulated by a modified Randles–Ershler equivalent electric circuit (inserted scheme, Figure 9a).[58,59] The constant phase elements were introduced to the model instead of capacitors to consider the non-uniform distribution of the film's thickness and its porous structure. The charge transfer resistance (R_{ct}) values obtained from the fitted spectra (**Figure S21**a, b) are shown in Figure 9 (a, b). These data show that the charge transfer resistance depends on the state of the polymer's charging for both materials in a similar way. The confined area with a decrease in the charge transfer resistance indicates the potential window where the polymers transition into a more conducting state during the redox processes. R_{ct} values for both polymers are of the same order of magnitude with that of pNiSalEn,[59] but pMTS shows a slightly higher minimum of R_{ct}, i.e., ~28–29 Ω cm^2 vs 3–4 Ω cm^2 for NiMeSalP(OH)En (Figure 9), testifying to the slower kinetics of the electrochemical reaction in pMTS. The parameter D_{eff} / L^2 that characterizes the diffusion rate of the charge carriers within the studied films can be calculated using a linear part of the i vs $t^{-\frac{1}{2}}$ plot and the Cottrell equation. For both polymers this parameter has the same order of magnitude as for pNiPhazoSalEn material and is about an order of magnitude lower than for pNiSalEn tested under the same conditions.[59] Based on these data, the electrochemical activity window is 0.2 – 0.6 V for the NiMeSalP(OH)En complex, and 0.4 – 0.65 V for the pMTS.

(a)   (b)
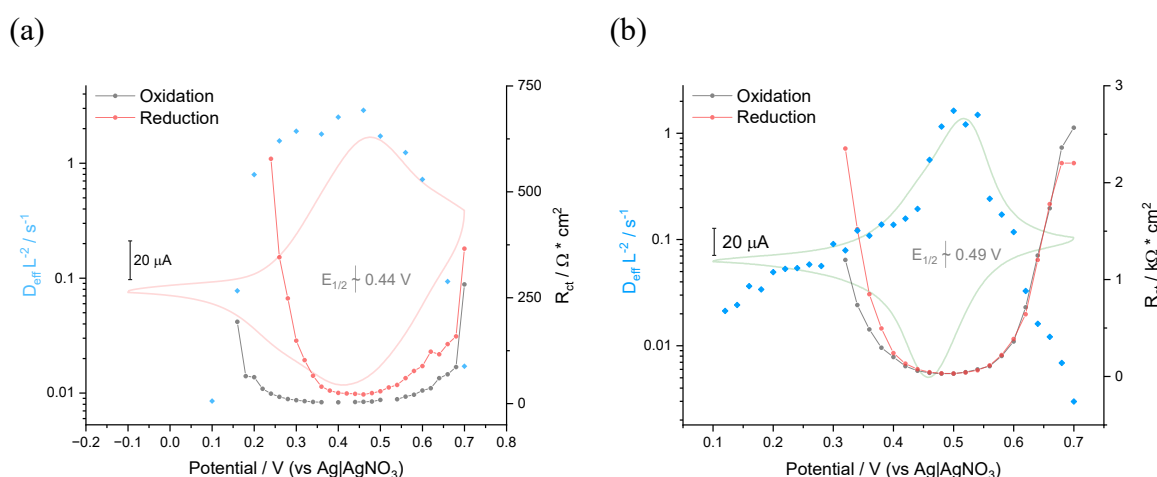
Figure 9. Charge transfer resistance and diffusion parameter dependencies on potential in oxidation and reduction processes for the GC electrode coated with the pNiMeSalP(OH)En (a) and pMTS (b) films in 0.1 M Et$_4$NBF$_4$ / CH$_3$CN. Cyclic voltammograms are plotted along with with the R_{ct} and diffusion data for ease of films' state interpretation.

WILEY-VCH

2.5.2. Conductance measurement

Operando electronic conductance of polymer films was studied using interdigitated electrodes (IDEs) using a bipotentiostat in CV mode. The dependence of the polymer's conductance on the applied potential (**Figure 10**) was found to be similar to that of pNiSalEns[47,48] and other conducting polymers,[60] showing a narrow conductivity window with a single peak at 0.29 V for pNiMeSalP(OH)En (Figure 10a) and two peaks at 0.29 V (backbone-related part) and 0.51 V (TEMPO related part) for pMTS (Figure 10b). However, the conductance of the investigated polymers is notably lower compared to polymers based on square-planar complexes (20 – 30 µS versus 0.3 – 2 mS). The trend of the conductance change for pMTS is identical to the trend for pDiTS measured in similar conditions with a maximum at ~0.50 V,[26] which shows that charge transfer is supported by the same mechanism in both polymers. Maximum conductance of pNiMeSalP(OH)En (Figure 10a) is also clearly visible in the conductance change profile of pMTS (Figure 10b), which indicates the separation of electronic conductivity profile at low scan rates. The presence of two conductance paths has a significant effect on the behavior of the material at low (below 1 mV s^{-1}) sweep rates, as discussed in the section 2.4. Since the conductivity of the systems is split into two parts, in the area where there is no backbone conductivity TEMPO has to transfer electrons according to a hopping mechanism without the participation of the conjugated polymer chain, which becomes an insulator.

(a)   (b)
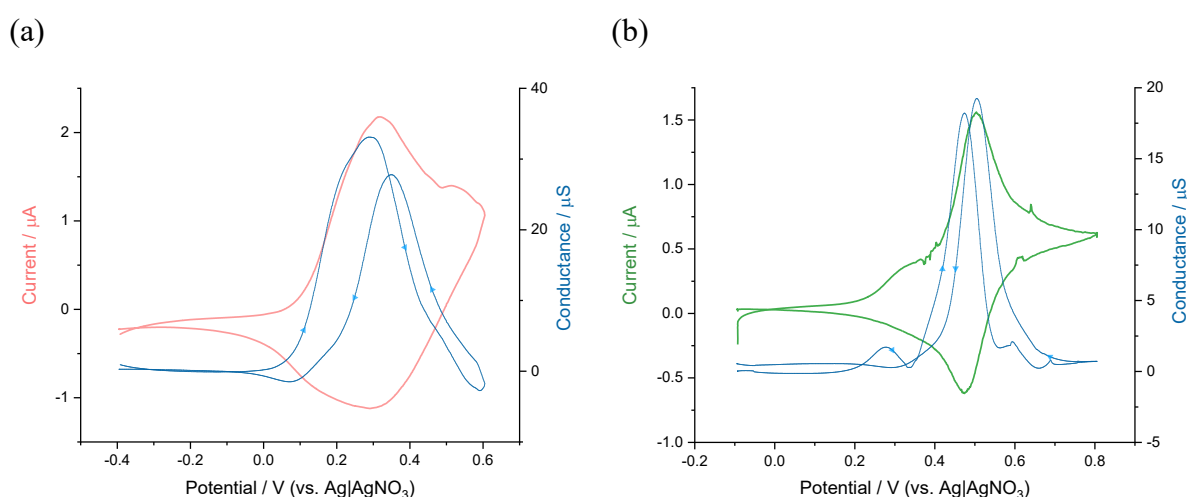
Figure 10. The conductance measured using interdigitated electrode arrays coated with the pNiMeSalP(OH)En (a) and pMTS (b) films in an 0.1 м Et$_4$NBF$_4$ / CH$_3$CN electrolyte recorded during CV with 0.5 mV s^{-1} scan rate and potential gap of 5 mV.
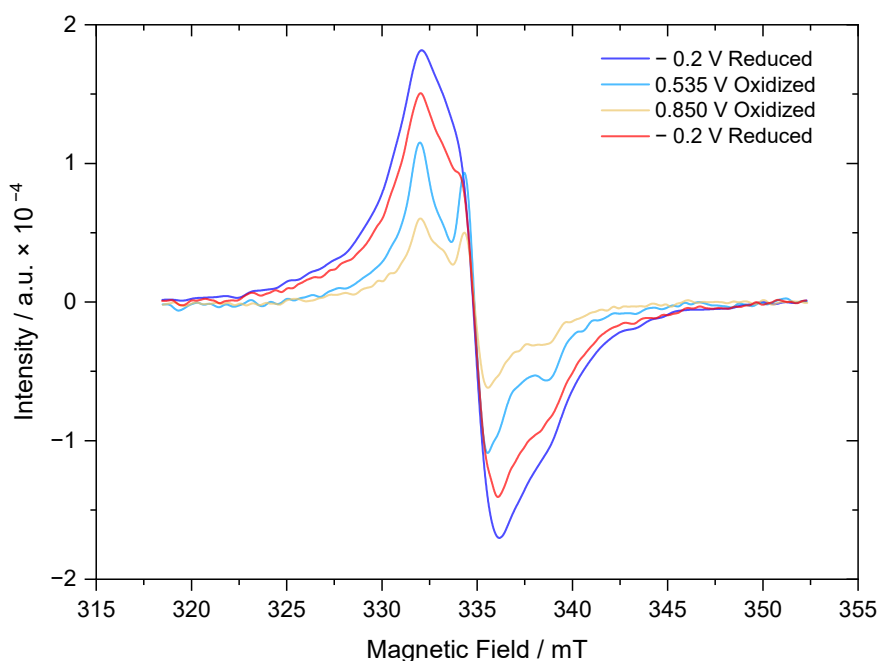
2.5.3. *Ex situ* CW-EPR

Sample preparation for electrochemical EPR analysis was conducted using a versatile on-substrate electrode setup as described earlier.[27] At first ex-situ CW-EPR study was attempted on pNiMeSalP(OH)En. However, no signal was observed in reduced (− 0.2 V), partially oxidized (0.1 – 0.4 V) or fully oxidized (0.7 V) polymer states at room temperature. In order to check the possibility of charge localization on the Ni atom, an analysis was carried out at 10 K, since the relaxation of the metal centered spin is usually fast and for similar complexes does not allow to see signals at RT.[61–63] There was no signal for thin (10 deposition cycles) and relatively thick (50 deposition cycles) films in both Ni- ($g \sim 2.3 – 2.2$) and organic radical-related ($g \sim 2.05 – 1.95$) regions of magnetic field. Considering the visual change and preservation of the color of the films during the experiment, we can assume that the achieved charge state was sufficiently stable. The EPR silent behavior in all charge states allows us to suggest that for the pNiMeSalP(OH)En conducting backbone, in contrast to planar SalEn-type complexes, the formation of quinone fragments rather than semiquinone radicals is preferable (**Figure 11**).

4,4 - dyhydroxybiphenyl   semiquinone radical (phenoxy radical - polaron)   quinone (bipolaron)
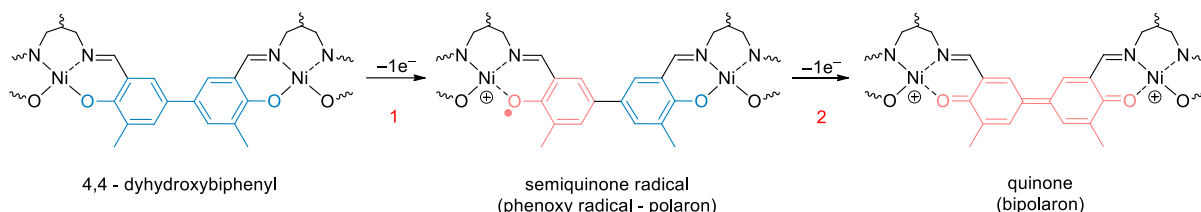
Figure 11. Representation of the step-by-step pMTS backbone oxidation.

Such a close arrangement of delocalized radicals can lead to antiferromagnetic coupling between the electron spins.[64] Another possible explanation for the lack of a signal could be the formation of intermolecular π-π stacking between adjacent chains — a π-dimeric charge transfer pathway, since in non-planar complexes, charge transfer along the polymer chain should be partially prohibited. It was found that the formation of antiferromagnetically coupled radicals is mainly characteristic of more electron rich ligands (containing CH_3O- or CH_3- substitutes)[34] which was used for NiMeSalP(OH)En construction. Thus, we also do not expect a contribution of backbone signals to the pMTS EPR spectrum and spin count. The same procedure was conducted for MTS. For the reduced pMTS state a single derivative

WILEY-VCH

broad lineshape in the CW-EPR can be seen (**Figure 12**). This single derivative is consistent with the high spin density in the film which leads to nearby nitroxides exhibiting exchange and/or dipolar couplings, leading to a loss of hyperfine and g-anisotropy which is usually found for immobilized nitroxide CW-EPR spectra.[27] Quantitative analysis of the CW-EPR spectrum gives the number of spins in the pMTS film to be 1.6×10^{15}. Then pMTS was slowly oxidized step by step from fully reduced (-200 mV vs Ag|AgNO$_3$) to fully oxidized (850 mV vs Ag|AgNO$_3$) states, each time holding the cell at the desired potential for 150 s before measuring the CW-EPR spectrum of the dry film. Oxidation of the cell to 535 mV results in a drop in the signal intensity and reveals to the spectrum structure characteristic of immobilized nitroxides, which do not exhibit strong spin-spin couplings to nearby nitroxides.

Figure 12. *Ex situ* spectra of continuous wave electron spin resonance for pMTS at RT at different potentials.

In previous studies involving di-nitroxide pDiTS,[27] two components were discerned in the in-situ and ex-situ CW-EPR spectra. These corresponded to the spin-spin coupled nitroxides that were electrochemically active and isolated islands of nitroxides which were neither spin-spin coupled nor electrochemically active. Hence the question here is whether the pMTS — which shows a strong signal corresponding to immobilized nitroxides — is electrochemically active or not. The pMTS film oxidized at 535 mV has 5.9×10^{14} spins in a paramagnetic state. Hence oxidizing to 535 mV leaves only 37% of the film in a paramagnetic state. Oxidizing

23

further to 850 mV (i.e., fully oxidized) leads to a drop in signal intensity again, suggesting that the immobilized nitroxide structure in pMTS is not necessarily electrochemically inactive, but rather that the more dilute nature of the pMTS film compared to the pDiTS film allows for the immobilized spectrum to be revealed at partial oxidation. At 850 mV, the number of spins decreased to 3.2×10^{14}, which is only 20% of the original spin count in the fully reduced state. Hence in ex-situ spectrochemical CW-EPR only around 80% of the nitroxide radicals in pMTS can be oxidized. This may be due to the appearance of isolated moieties that cannot be completely oxidized, or internal charge transfer between the polaron and TEMPO$^+$, which maintains a certain constant concentration of TEMPO radicals.[28,29] Subsequent film reduction of pMTS to −200 mV (vs Ag|AgNO₃) leads to spectral line structure that recovers partially to the original lineshape, with the presence of the spectrum structure of the oxidized state still noticeable for the reduced state. The number of spins in the fully reduced pMTS after the full ex-situ study shows a spin count of 1.3×10^{15}, which is 79% of the starting spin count. In summary, spectroelectrochemical ex-situ CW-EPR reveals that 80% of nitroxide spins in pMTS are electrochemically active when oxidizing pMTS from −200 mV to 850 mV, and that reducing the pMTS again leads to a 20% decrease in the number of spins (compared to the initial reduced state spin count) which are either lost from the film during its partial dissolution or remain in an oxidized and therefore EPR silent state.

2.5.4. UV-vis spectroelectrochemistry (SEC)

SEC analysis allowed us to view the obtained polymer films in the framework of the polaron-bipolaron model, to monitor the emergence and dissipation of charge-carrying pseudoparticles in the polymers upon oxidation and reduction, and to verify whether the introduction of an organic radical species into the film modified the electronic transformations within the polymer backbone.

The results of the SEC analysis are presented in **Figure 13** and **Figure S22**. Several UV–visible region bands appear during the polymers oxidation that show different dependencies on applied potential. As seen in the absolute spectra (referenced to the background clean ITO/glass electrode in electrolyte) (Figure S22a, b), the polymers pNiMeSalP(OH)En and pMTS show similar spectral behavior during oxidation with a small spread of band maxima of ~5–10 nm. These data provide accurate values of absorbance band maxima and were used for DCVA representation. The difference UV spectra (the reduced polymer state was used as a

WILEY-VCH

reference point) were used to visualize the changes of the electronic bands along with potential (colormaps) and to calculate the molar extinction coefficients (**Figure S23, S24**). For both polymers several most cited bands were isolated and linked with potential (Figure 13c, d). The λ_{max} values of the observed absorbance bands are summarized in **Table 1**. Oxidation of both polymers is accompanied by a decrease of absorbance at $\lambda \approx 350$ nm, along with the emergence and growth of new bands at $\lambda \approx 380 - 420$ nm and a couple of broad bands with maxima at 690 nm and 940 nm. These new growing bands reach maximum absorbance at $E \approx 0.35$ V. At higher oxidation states, the intensity of the band at $\lambda \approx 350$ nm continues to decrease for both polymers, while the other bands only begin to decrease, and a new band at $\lambda \approx 490$ nm shows a sharp increase until the end of the oxidation. The appearance of this new band is also accompanied by the appearance of an isosbestic point at 404–406 nm. In the cathodic scan, these absorbance changes are reversed.

(a)

(b)

(c)

(d)
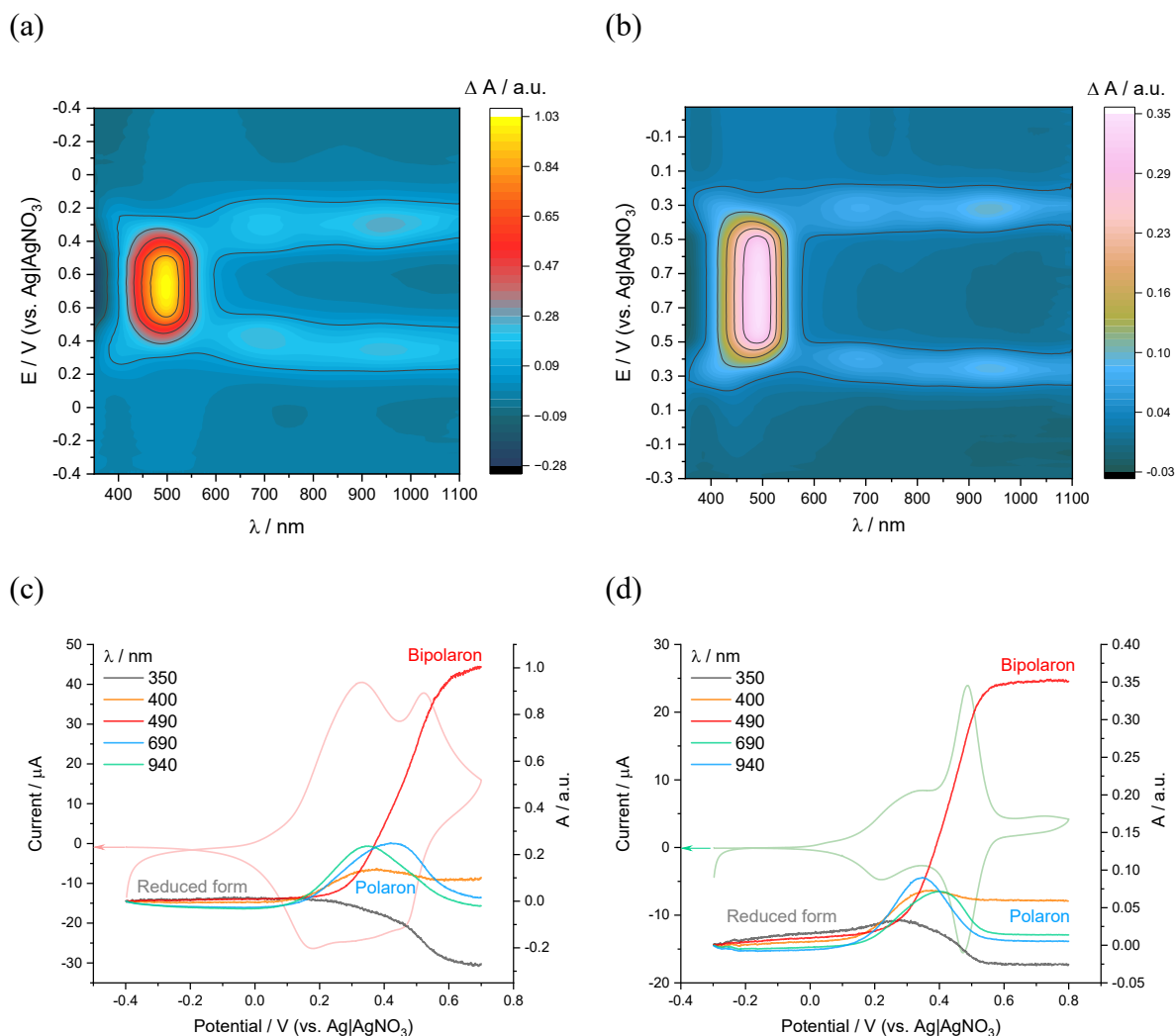
Figure 13. Differential *operando* UV-Vis / CV spectra of pNiMeSalP(OH)En (a) and pMTS (b) at a sweep rate of 1 mVs^{-1}; maximum of characteristic polaron-bipolaron spectral bands as a function of potential for the pNiMeSalP(OH)En (c) and pMTS (d) systems.

The combination of the Beer–Lambert and Faraday laws allows one to estimate the molar extinction coefficient ($\varepsilon(\lambda)$/ M^{-1} cm^{-1}),[65–67] which can be used for proper band assignment. The coefficients were calculated from the slopes of the linear parts of d$A(\lambda)$ vs Q plots (Figure S23, S24) and are summarized in Table 1. The ε-values in the range >1000 M^{-1} cm^{-1} are typical for electronic transitions between the states with large contributions from ligand orbitals.[67] As the observed electronic bands are not visible for the reduced polymer state, they can be assigned to the electronic transitions between the new electronic states formed during the polymer oxidation, for example during the formation of a delocalized cation-radical or a polaron. The observed bands were also detected for other Cu-,[68] Pd- [69] or Ni-

26

WILEY-VCH

[34,65,67,70] based SalEn-type materials and TEMPO-modified NiSalEn-based polymer.[26] The polaronic model developed for organic conductors[71] was previously employed by Hillman et al. for the examination of the polaronic states in SalEn-type materials,[65,67–69] and thus we use it here for proper bands assignment.

Table 1. Electronic bands and their respective molar extinction coefficients (ε) for polymers during oxidation.

Polymer	λ_{max} [nm]	$\varepsilon \times 10^{-4}$ [M^{-1} cm^{-1}]	Energy [eV]
pNiMeSalP(OH)En	350	0.30	3.54
	400	0.29	3.10
	490	1.24	2.53
	690	0.43	1.79
	940	0.53	1.32
pMTS	350	0.21	3.54
	400	0.65	3.10
	490	2.70 (0.81[a])	2.53
	690	0.73	1.79
	940	1.0	1.32

[a] calculated from the area of 0.5 V

After the electron is withdrawn upon oxidation, the new polaronic bonding and antibonding states can be formed. The authors of the above-mentioned works assumed that the polaronic states formation led to three possible electron transitions with energy below that of the intervalence band transition (**Figure 14**): W_1 — charge transfer from the valence band to the bonding polaron band, W_2 — the transfer from the valence band to the antibonding polaron band, W_3 — the transfer between bonding and antibonding polaron energy levels.[67] These transition energies are related to each other and to the intervalence band (W_I) as follows: $W_1 + W_3 = W_2$, and $W_1 + W_2 = W_I$, in the case of symmetric distribution of the gap-state energy levels approximation. Further oxidation can lead to the bipolaron formation if this pairing charge state is available. As the bands at 400 nm, 690 nm, and 940 nm have roughly the same A vs E profiles (Figure 13c, d) they can be associated with the same charge carriers. Thus, for both polymers: the electronic bands with the highest energy transition at λ_{max} around 350 nm (>3.5 eV) can be assigned to the intervalence band, W_I, since they decrease in intensity upon

polymer oxidation; the bands at $\lambda \approx 400$ nm (3.1 eV) are assigned to the charge transfer from the valence band to the antibonding polaron level — W$_2$; the bands at $\lambda \approx 690$ nm (1.8 eV) are assigned to the transition between the bonding and the antibonding polaron levels — W_3; the bands at $\lambda \approx 940$ nm (1.4 – 1.2 eV) are related to the transition from the valence band to the bonding polaron level — W_1. As the polaron population and, accordingly, polaronic states are rising along with polymer oxidation, the related bands increase in intensity. This assignment perfectly matches the relationship between the transition energies (Figure 14) $W_1 + W_3 = W_2$, and $W_1 + W_2 = W_I$, though the W$_I$ value is slightly lower than expected. This can be due to the uncertainty of W_I estimation. Since ITO/glass substrates were used in this work, the region below 350 nm is not available for analysis due to the strong substrate absorption in this region. Nevertheless, for nickel complexes of the SalEn type with various substituents, it was shown that W_I lies in the region of 280 – 330 nm, which corresponds to the energy of 3.7 – 4.4 eV.[34] In this work, the band at 350 nm, although not a peak value, is still suitable for analyzing the behavior of the polymer during oxidation. At potentials above 0.3 V the intense band with the molar extinction coefficient of two-to-three times higher (Table 1) than for others appears at $\lambda = 490$ nm (2.5 eV) and shows a different A vs E profile with respect to all the other bands (Figure 13c, d). During the polymer oxidation, a new state of electronic π system (bipolaron) can form due to the detachment of the second electron from the polaron level. Thus, the new band at 490 nm can be assigned to the charge transfer transitions from metal to π system formed through the quinoid between the two phenyl rings.[26,34,65,67,72] This assignment is also confirmed by the fact that an isosbestic point between the phenoxyl radical bands appears (Figure 11) and all other bands decrease after the appearance of the band at 490 nm, which is associated with a decrease in the population of polarons during the bipolaron formation (Figure 13c, d).
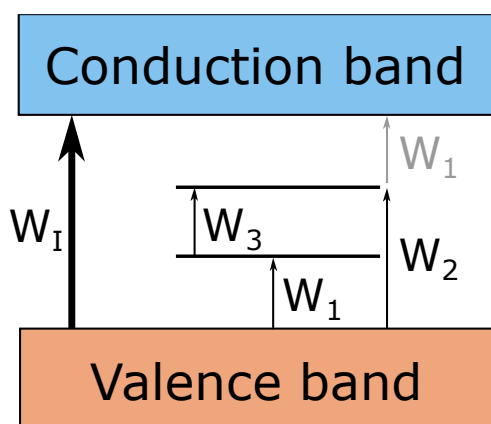
Figure 14. Energy scheme of electron transfers in the studied materials.

The polymers have identical UV-vis spectra evolution during charge/discharge, and the only differences are slight variations in the maximum band values (~10 nm) as a consequence of the change of the structure from the alcohol to the TEMPO-succinyl linker-modified diimine bridge. Such substituent replacement does not lead to a significant change in electronic structure as observed for substituents in phenyl rings.[34] Thus, the structure of the complex has an overwhelming effect on the distribution of electronic bands. Deviation of complex structures from planarity can lead to the formation of "charge-trap" regions that do not have electrical activity. Thus, at reduced state the broad low intensity peak at 690 nm can be noticed, which corresponds to the trapped polarons after the polymer formation (Figure S22). In contrast to other SalEn-type complexes,[34] in this case, the bands corresponding to the main electron transitions are narrower and more pronounced (Figure S22a, b). The narrowing of the band at > 950 nm, which corresponds to phenolate-to-phenoxyl radical (ligand-to-ligand) charge transfer and indicates realization of conductance along the polymer chain,[65] is also noticeable. Such a blue shift from >1000 nm for planar complexes based on ethylenediamine bridge to ~ 950 nm for propyl-bridged one can be the evidence of the lower delocalization length of the unpaired electrons on the phenolate moieties of the ligand.[34] This can be caused by the distortion of the geometry of the complex and less involvement of metal d orbitals in the π-system of the complex.[73] We observed an extremely small gap (Figure 13c, d) between potentials (~100 mV) of the polaron and bipolaron formation, which may also be a consequence of low charge delocalization, low efficiency of intermolecular charge transfer and rather formation of the quinone fragment than semiquinone radicals. This is in good agreement with the low values of electronic conductivity that were obtained using IDEs (Figure 10a) and the absence of an EPR signal during the oxidation of pNiMeSalP(OH)En.

WILEY-VCH

The small blue shift of the 690 nm and 940 nm bands (Figure S22a, b) with increasing potential was also noticed. Rise in polaron and bipolaron concentrations should confine the delocalization length causing spectral blueshift.[74] This behavior can also be caused by π-dimer formation between two adjacent phenoxyl fragments.[34,75,76] In the case of the bipolaron-related 490 nm band we observed a weak red shift, perhaps caused by shortening distance and strengthening mutual repulsion between the same type chromophores with the rise of their concentration.[74] The presence of the bands at $\lambda_{max} \sim 460–470$ nm associated with TEMPO radical and cation states in the reduced and oxidized states of the polymer, respectively,[12,77] were not observed at the absolute spectra for pMTS (Figure S22b). However, the extinction coefficient for the TEMPO (10.5–20.3 M^{-1} cm^{-1}) group is much lower than that for NiSalEn-type molecules ($1–10\times10^3$ M^{-1} cm^{-1})[33,67,77] which leads to the concealment of the low-intensity bands of TEMPO/TEMPO$^+$. For this reason, the molar extinction coefficient calculated from the slope at ~0.5 V region is significantly underestimated (Table 1), since the charge is spent on the TEMPO/TEMPO$^+$ transformation without a contribution to the absorption value.

2.5.5. Derivative cyclic voltabsorptometry (DCVA)

Now that we know the relationship between the electronic bands and the moieties they are related to, we can move on to the link between the electrochemical signal and the spectral bands. From A vs E plots (Figure 13c, d) and DCVA data for the main electronic bands (**Figure S25**, **S26**), the CV peaks can be easily assigned to the electroactive species formed during the oxidation. As we can see, the first pair of oxidation/reduction peaks (~0.25 V) of both polymers is related to the activity of polarons, which is responsible for the conductivity of the organometallic backbone (Figure 10). The band at 490 nm corresponding to the appearance of a bipolaron can be attributed to the second oxidation peak at ~0.5 V of pNiMeSalP(OH)En (Figure S25c), which is hidden by the activity of TEMPO groups in pMTS (Figure S26c). It is worth mentioning that all the highlighted bands change by absorbing the charge and correspond to the electrochemical processes, thus no additional chemical processes were found between the stages of electrochemical oxidation / reduction. Raw DCVA data (dA/dt vs E) can be easily converted to a voltabsorptogram using the equation [33]:

$$I = S \cdot n \cdot F \, (\mathrm{d}A_1/\mathrm{d}t \cdot 1/\varepsilon_1 + \mathrm{d}A_2/\mathrm{d}t \cdot 1/\varepsilon_2 + \ldots + \mathrm{d}A_\mathrm{n}/\mathrm{d}t \cdot 1/\varepsilon_\mathrm{n}).$$

A comparison of CV data and voltabsorptograms for both polymers is presented in **Figure 15**a, b. The voltabsorptograms and voltammograms perfectly match. The voltabsorptogram of pNiMeSalP(OH)En contains the same number of peaks and values of peak potentials as the CV curve. As most physical data for both polymers are the same, the same shape of the voltabsorptogram can be assumed for pMTS. Based on these data some valuable information can be calculated. The maximum theoretical capacity of pMTS (126.2 mA h g^{-1}) was calculated based on the participation in the electrochemical process of three electrons (polaron-bipolaron and TEMPO/TEMPO^{+}) per monomer unit. Thus, the ratio between the areas under the CV curves corresponding to the polaron-bipolaron process and the whole process in pMTS should be 2:3. Based on the data obtained, this ratio was 2:3.2, which gives 1.66 electrons involved in the electrochemical activity from the monomer unit and 1 electron from TEMPO per monomer unit. Thus, the theoretical capacity for 2.66 electrons is 112 mA h g^{-1}. It should be noted that the specific capacity obtained for pNiMeSalP(OH)En was 96.6 mA h g^{-1} (1.38 electrons per monomer unit) which is 69% of the maximum theoretical capacity of 139.9 mA h g^{-1}. Considering this number of electrons and the ratio between the SalEn and TEMPO components obtained above, we can assume that during pMTS oxidation 1.38 electrons are consumed from the metalorganic chain and 0.83 electrons from TEMPO per monomer unit. This ratio reduces the theoretical capacity to 93 mA h g^{-1} (2.21 electrons), which is in excellent agreement with the obtained capacity for pMTS (94.7 mA h g^{-1}, 2.25 electrons). The slight decrease in TEMPO activity, which we discussed in section 2.4, and the growth of the difference between TEMPO cathodic and anodic peaks at low scan rates may be due to the relative position of the polaron-bipolaron band and the TEMPO oxidation peak (Figure 15c).

WILEY-VCH

(a)

(b)

(c)

(d)
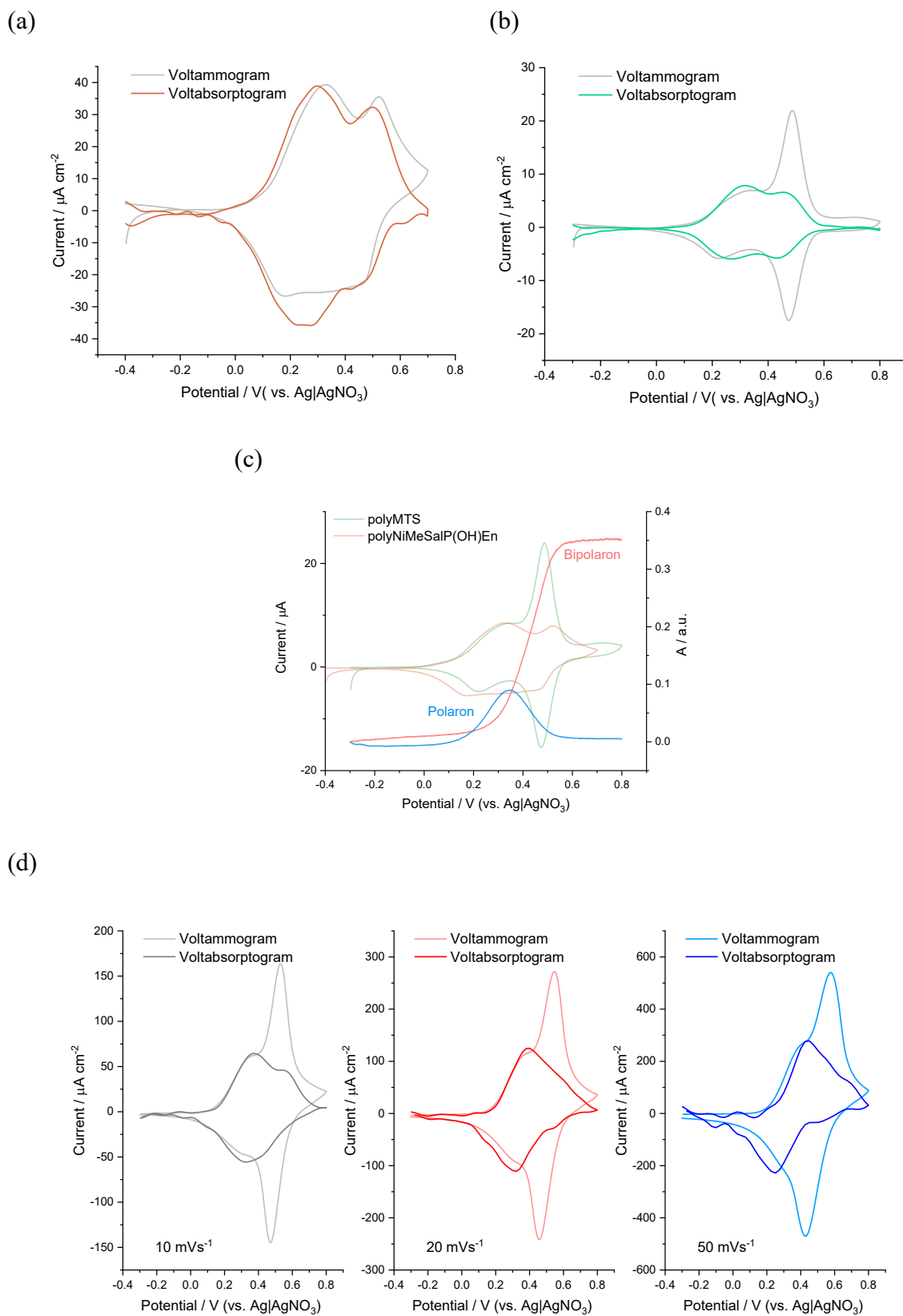
Figure 15. Comparison of voltammograms and voltabsorptograms for pNiMeSalP(OH)En (a) and pMTS (b) observed at the potential scan rate of 1 mV s^{-1}; Comparison of CV curves and

polaron-bipolaron bands changing (c); comparison of voltammograms and voltabsorptograms for pMTS observed at the different potential scan rates (d).

At low sweep rates, at ~0.45 V, i.e., before the onset of TEMPO oxidation, a significant decrease occurs in the population of polarons, and, consequently, in the conductivity (Figure 10). Therefore, at low scan rates, charge transfer from TEMPO to SalEn chain can be prohibited. Dynamic analysis, on the other hand, shows a broadening of the window of electroactivity (expansion of the zone of the existence of the polaron) with an increase in the scan rate (Figure 15d and **Figure S27**). This may be due to the non-zero resistance to charge transfer in film and finite time of this transfer. Polaron zone expansion allows TEMPO to use the chain's conductivity during recharging at a higher scan rate. This feature is important in connection with the efficiency of the material, which is mainly influenced by the "non-optimality" of the structure of the monomer complex, characterized by incomplete overlap of the working potential windows of its components. In this case kinetics of polaron formation and their transition to bipolarons becomes important for maintaining the film conductivity in the range of potentials, corresponding to pendant groups redox reaction.

2.5.6. DFT geometry optimization for di- and tetramers during step-by-step oxidation

DFT calculations for positively charged complexes were performed to demonstrate the mechanism of the stepwise electron withdrawal (**Figure S14**), which mimics the actual oxidation process. Monomer complexes served as basic models, while dimers and tetramers could provide a more detailed description of electron withdrawal. The removal of the first half-electron per monomer unit primarily involved the Ni-ligand chain and resulted in the formation of a non-zero spin density region between the two metal sites. For tetramers in the same oxidation state two such regions were formed, resulting in a spin density distribution (**Figure S15**) close to that expected in the case of polaron formation. Further oxidation of complexes up to the one-electron-per-unit level does not involve either of the TEMPO groups and appears to increase the electronic connectivity of the oligomer molecule, with spin density being distributed more or less evenly along the entire chain. The electronic effects observed at this stage of oxidation can be assigned to the formation of bipolarons. Further oxidation to the 1½ electrons-per-unit level did not significantly affect the free-radical substituents (Figure S14, S15), which were simultaneously charged only upon final oxidation

This is a Submitted version before peer review.
Published version available at 10.1002/marc.202400074

WILEY-VCH

to two electrons-per-unit. The changes in the electronic structure caused by oxidation are accompanied by structural transformations in the oligomer chain. Upon initial oxidation, the angle between adjacent monomer units in dimers, which is equal to 32–33 degrees for neutral molecules, decreases to 17 – 19 and remains almost constant until the final stage of oxidation, when it increases to 22 – 23 degrees. In tetramers one can even distinguish between polaron-like and bipolaron-like structures, since the former display a noticeable difference in the angles between monomer units for strongly and weakly perturbed fragments (typically, less than 24 degrees inner polaron- and bipolaron-like fragments vs. 30 – 31 degrees outer polarons). The overall process of MTS oxidation is generally similar to NiMeSalP(OH)En precursor complex (**Figure S16**), including the distinct two-stage oxidation of the oligomer chain. Despite this slight difference in angles between phenyl rings in these complexes, we did not observe a significant difference in the electrochemical behavior of their Salen moieties. However, for both complexes the calculated Ph-Ph angles are significantly larger (32 – 37 degrees) than for square planar complexes based on ethylenediamine (Table S1). Compared to square planar complexes we observed notable changes in electrochemical, spectral and physical (morphology, SEM) properties. Thus, due to deviation from a square planar complex structure due to the presence of a triatomic imine bridge bearing an out-of-plane -O- fragment, compare with polymers based on planar complexes we noticed a strong decrease in stability[26,57,78] and conductivity,[48] as well as more unbound films formation[25,40–42] and anomalously small gap between the polaron and bipolaron formation potentials.[34]

2.5.7. Open circuit potential and UV-vis spectra relaxation

Given the rather large potential difference between the oxidation/reduction peaks of the TEMPO and SalEn components we can consider pMTS as a semi-optimal hybrid system, in which internal charge transfer processes may occur. To investigate this process, open circuit potential (OCP) relaxation coupled with UV-vis spectroscopy was monitored for pNiMeSalP(OH)En (**Figure 16**a) and pMTS (Figure 16b). The polymers were charged to 0.8 V and then held at this potential for 30 s.

(a)

(b)

(c)
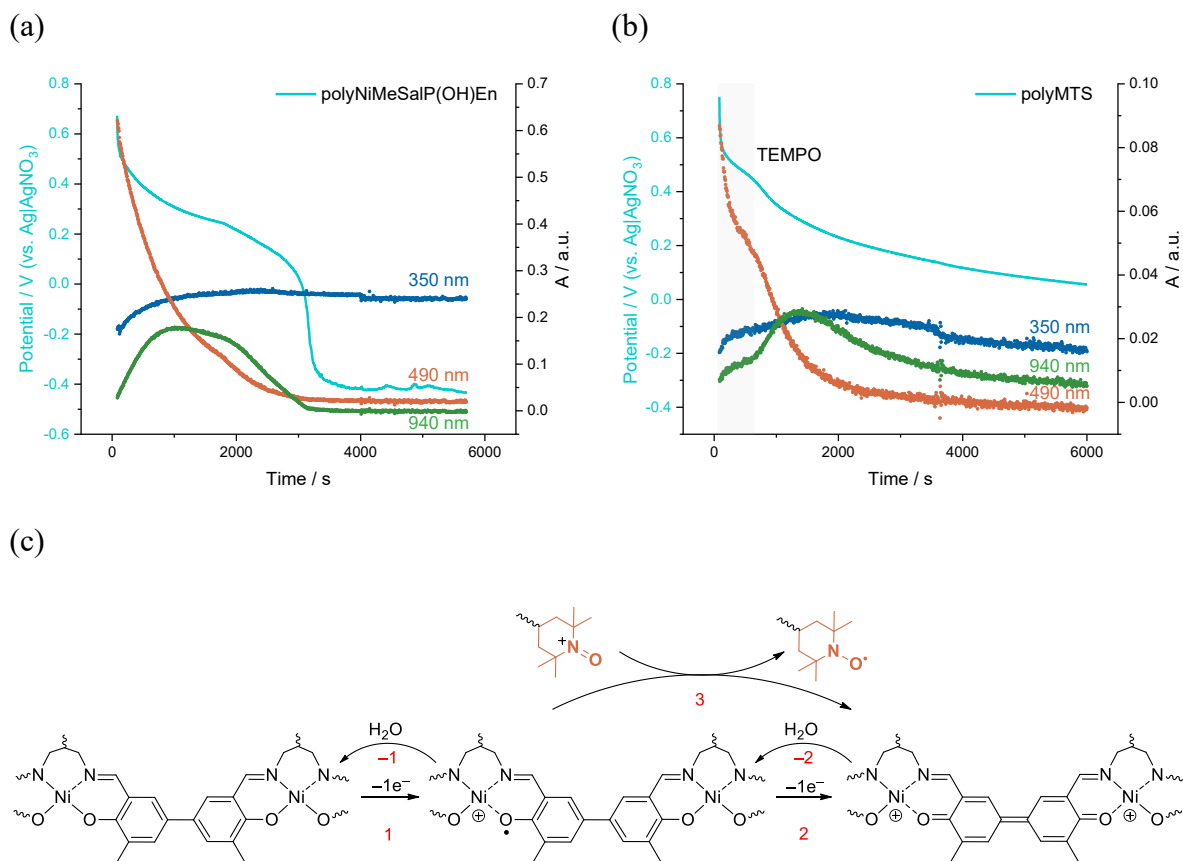
Figure 16. Relaxation of the open circuit potential and the main spectral bands in the open circuit for pNiMeSalP(OH)En (a) and pMTS (b); Scheme of the side reaction of bipolaron with water and TEMPO$^+$ particles (c).

The OCP was then monitored for ~ 4000–6000 s. Relaxation of the precursor polymer is a two- step process in which a slow drop in potential to 0.25 V is observed, followed by a sharp drop in potential to − 0.4 V (Figure 16a). This behavior can be associated with both the gradual dedoping of the material[28] and side reactions of the polymer with residual water in the supporting electrolyte.[57] An analysis of the spectral curves showed that during relaxation of pNiMeSalP(OH)En (Figure 16a) a rapid decrease in the bipolaron band is observed, while for the polaron bands an initial increase and then a decrease are observed. The sharp drop in potential after 1800 seconds suggests that the material became totally discharged and the potential dropped to the equilibrium ITO/electrolyte system potential. The relaxation of the pMTS consists of two steps, the discharge of TEMPO groups to 0.5 V and consequent discharge of the polymer backbone (Figure 16b). The relaxation of the spectral lines for pMTS (Figure 16b) is generally similar to the spectral relaxation pattern of the precursor polymer, but contains a small tail shape feature on the bipolaron band relaxation profile in the

WILEY-VCH

first 500 s. This time correlates with a plateau in the OCP relaxation pattern. Most likely, the same processes occur for pMTS as for pNiMeSalP(OH)En, but the discharge of the conducting backbone may be accompanied by intramolecular electron transfer to the TEMPO group. We assume the presence of a series of interactions between the backbone and water, the reduction of bipolarons to polarons, and the sequential oxidation of polarons to bipolarons by oxidized TEMPO groups (Figure 16c). This process keeps the bipolaron levels stable until the TEMPO groups are fully reduced. The polymer then continues to discharge, accompanied by a drop in the bipolaron and polaron bands. The potential stabilization in the case of pMTS may be associated with a more pronounced steric loading of the polymer, preventing the free movement of water molecules deep into the polymer and possible presence isolated from backbone charged TEMPOs.

3. Conclusion

In this study, we have successfully synthesized and characterized a novel redox-conducting polymer, pMTS, by incorporating TEMPO moieties into the diimino-bridge of a NiSalEn-type complex. Our findings were compared with its TEMPO-free counterpart, pNiMeSalP(OH)En. Through a combination of experimental data and DFT modeling, we have gained valuable insights into the structure, morphology, and electrochemical behavior of these polymers. DFT calculations with previously reported X-ray crystal diffraction data revealed that the choice of 2-hydroxypropyliden imine bridge for ligand design resulted in a deviation of the molecular geometry from planar to tetrahedral. This structural difference significantly influenced the morphology and properties of the resulting polymeric films. The introduction of TEMPO-bearing linkers did not induce significant changes in the molecular geometry but had a substantial impact on film uniformity. The addition of TEMPO led to several notable modifications in film properties. It introduced a "solvate coulombic shield" that influenced mass and charge transfer processes during polymer formation and cycling, effectively protecting the polymer backbone from side reactions. As a result, pMTS exhibited enhanced stability, retaining 47% of its initial capacity after 500 cycles, compared to pNiMeSalP(OH)En, which retained only 17%. Furthermore, pMTS demonstrated an increased specific capacity of up to 13%, reaching 71 mA h g^{-1} at a high current rate of 20C. However, the TEMPO-modified material has a lower efficiency and capacity at lower scan rates, warranting additional in-depth investigation of the materials using a combination of

electrochemical and spectral methods. Electrochemical impedance spectroscopy confirmed comparable diffusion constants and charge transfer resistances for both materials, consistent with previous studies on SalEn-based polymers. Electrical conductance measurements revealed a wide conductivity window for both materials, with pMTS exhibiting a split profile due to the transition from conducting backbone charge carriers in pNiMeSalP(OH)En to TEMPO in pMTS. EPR data indicated efficient diamagnetic polaron coupling during backbone oxidation, rendering it EPR silent. Achieving a high degree of TEMPO oxidation in pMTS proved challenging, likely due to charge transfer limitations due to decrease of backbone conductivity at high oxidation potentials. UV-Vis spectroscopy showed that the charge transfer is mainly provided by polaron and bipolaron pseudoparticles. *Operando* UV-Vis studies during CV cycling highlighted the relationship between the materials charge state and the population of polarons and bipolarons. Notably, UV-Vis studies at lower scan rates unveiled an edge effect, with a reduction in polaron population just before TEMPO oxidation onset, resulting in a slight loss of conductance and lower charge transfer efficiency. Coulometric studies paired with the spectral data indicated that during oxidation 0.83 electrons are originating from TEMPO and 1.38 electrons from the backbone per monomer unit. Open-circuit potential relaxation experiments suggested the involvement of oxidized TEMPO moieties in internal charge transfer side reactions, explaining the efficiency loss at lower scan rates.

In conclusion, this study underscores the critical role of molecule design, which should be tailored to the specific task at hand. For tasks requiring enhanced stability and minimal side reactions, optimal systems with perfectly overlapping working potential windows are the preferred choice. In addition, polymers based on more stable square-planar complexes, which have the advantage of low solubility, and thoroughly purified and dried solvents, which should minimize the activity of side processes, can be used. Conversely, semi-optimal systems such as MTS may be more suitable for catalytic reactions. The profound influence of molecular structure on properties paves the way for further investigation of similar systems, both in terms of mechanistic peculiarities and direct applications. For studies of materials with transient properties, such as a hybrid of a redox and a conducting polymer, an unconventional non-planar structure such as the one developed here is highly appropriate. To explore semi-optimal systems or to study linker effects, it is recommended to increase the electronegativity induction and the mesomeric effect of linkers and substituents to bring the polymer activity

WILEY-VCH

closer to that of TEMPO. These findings are expected to benefit future research in related areas and may have implications for the development of advanced electroactive materials.

Supporting Information

Contains additional experimental data and Experimental Section/Methods section. Supporting Information is available from the Wiley Online Library or from the author.

WILEY-VCH

References

[1]   K.-A. Hansen, J. P. Blinco, *Polym. Chem.* **2018**, *9*, 1479.

[2]   S. Muench, A. Wild, C. Friebe, B. Häupler, T. Janoschka, U. S. Schubert, *Chem. Rev.* **2016**, *116*, 9438.

[3]   J. Kim, J. H. Kim, K. Ariga, *Joule* **2017**, *1*, 739.

[4]   D. Larcher, J.-M. Tarascon, *Nat. Chem.* **2015**, *7*, 19.

[5]   C. Friebe, U. S. Schubert, *Top. Curr. Chem.* **2017**, *375*, 19.

[6]   T. Janoschka, M. D. Hager, U. S. Schubert, *Adv. Mater.* **2012**, *24*, 6397.

[7]   K. Nakahara, K. Oyaizu, H. Nishide, *Chem. Lett.* **2011**, *40*, 222.

[8]   J. Lutkenhaus, *Science (80-.).* **2018**, *359*, 1334.

[9]   C. Friebe, U. S. Schubert, **2019**, pp. 65–99.

[10] K. Nakahara, S. Iwasa, M. Satoh, Y. Morioka, J. Iriyama, M. Suguro, E. Hasegawa, *Chem. Phys. Lett.* **2002**, *359*, 351.

[11] S. Muench, P. Gerlach, R. Burges, M. Strumpf, S. Hoeppener, A. Wild, A. Lex-Balducci, A. Balducci, J. C. Brendel, U. S. Schubert, *ChemSusChem* **2021**, *14*, 449.

[12] K. Zhang, Y. Hu, L. Wang, J. Fan, M. J. Monteiro, Z. Jia, *Polym. Chem.* **2017**, *8*, 1815.

[13] S. Komaba, T. Tanaka, T. Ozeki, T. Taki, H. Watanabe, H. Tachikawa, *J. Power Sources* **2010**, *195*, 6212.

[14] R. Rohan, M.-K. Hung, Y.-F. Yang, C.-W. Hsu, C.-K. Yeh, Y.-L. Chang, J.-T. Lee, *ACS Appl. Polym. Mater.* **2022**, *4*, 2365.

[15] Y. Chen, Y. Zhang, X. Liu, X. Fan, B. Bai, K. Yang, Z. Liang, Z. Zhang, K. Mai, *Macromol. Rapid Commun.* **2018**, *39*, DOI 10.1002/marc.201800195.

[16] K. Takahashi, K. Korolev, K. Tsuji, K. Oyaizu, H. Nishide, E. Bryuzgin, A. Navrotskiy, I. Novakov, *Polymer (Guildf).* **2015**, *68*, 310.

[17] A. A. Vereshchagin, A. Y. Kalnin, A. I. Volkov, D. A. Lukyanov, O. V. Levin, *Energies* **2022**, *15*, 2699.

[18] L. Bugnon, C. J. H. Morton, P. Novak, J. Vetter, P. Nesvadba, *Chem. Mater.* **2007**, *19*, 2910.

WILEY-VCH

[19] M. Suguro, S. Iwasa, Y. Kusachi, Y. Morioka, K. Nakahara, *Macromol. Rapid Commun.* **2007**, *28*, 1929.

[20] M. Aydın, B. Esat, Ç. Kılıç, M. E. Köse, A. Ata, F. Yılmaz, *Eur. Polym. J.* **2011**, *47*, 2283.

[21] L. Xu, F. Yang, C. Su, L. Ji, C. Zhang, *Electrochim. Acta* **2014**, *130*, 148.

[22] P.-O. Schwartz, M. Pejic, M. Wachtler, P. Bäuerle, *Synth. Met.* **2018**, *243*, 51.

[23] L. Xu, L. Ji, G. Wang, C. Zhang, C. Su, *Ionics (Kiel).* **2016**, *22*, 1377.

[24] C. O'Meara, M. P. Karushev, I. A. Polozhentceva, S. Dharmasena, H. Cho, B. J. Yurkovich, S. Kogan, J.-H. Kim, *ACS Appl. Mater. Interfaces* **2019**, *11*, 525.

[25] S. N. Eliseeva, E. V. Alekseeva, A. A. Vereshchagin, A. I. Volkov, P. S. Vlasov, A. S. Konev, O. V. Levin, *Macromol. Chem. Phys.* **2017**, *218*, DOI 10.1002/macp.201700361.

[26] A. A. Vereshchagin, D. A. Lukyanov, I. R. Kulikov, N. A. Panjwani, E. A. Alekseeva, J. Behrends, O. V. Levin, *Batter. Supercaps* **2021**, *4*, 336.

[27] I. Kulikov, N. A. Panjwani, A. A. Vereshchagin, D. Spallek, D. A. Lukianov, E. V. Alekseeva, O. V. Levin, J. Behrends, *Energy Environ. Sci.* **2022**, *15*, 3275.

[28] F. Li, S. Wang, Y. Zhang, J. L. Lutkenhaus, *Chem. Mater.* **2018**, *30*, 5169.

[29] F. Li, D. N. Gore, S. Wang, J. L. Lutkenhaus, *Angew. Chemie Int. Ed.* **2017**, *56*, 9856.

[30] J. Qu, T. Fujii, T. Katsumata, Y. Suzuki, M. Shiotsuki, F. Sanda, M. Satoh, J. Wada, T. Masuda, *J. Polym. Sci. Part A Polym. Chem.* **2007**, *45*, 5431.

[31] S. Bahceci, B. Esat, *J. Power Sources* **2013**, *242*, 33.

[32] D. A. Lukyanov, V. V. Sizov, A. I. Volkov, E. V. Beletskii, A. N. Yankin, E. V. Alekseeva, O. V. Levin, *Molecules* **2022**, *27*, 8798.

[33] V. V. Sizov, M. V. Novozhilova, E. V. Alekseeva, M. P. Karushev, A. M. Timonov, S. N. Eliseeva, A. A. Vanin, V. V. Malev, O. V. Levin, *J. Solid State Electrochem.* **2015**, *19*, 453.

[34] E. Dmitrieva, M. Rosenkranz, J. S. Danilova, E. A. Smirnova, M. P. Karushev, I. A. Chepurnaya, A. M. Timonov, *Electrochim. Acta* **2018**, *283*, 1742.

[35] A. I. Volkov, R. V. Apraksin, E. A. Falaleev, J. V. Novoselova, Y. A. Volosatova, D. A. Lukyanov, E. V. Alekseeva, O. V. Levin, *Electrochim. Acta* **2022**, *425*, 140750.

[36] D. A. Lukyanov, A. A. Vereshchagin, E. V. Beletskii, A. B. Atangulov, A. N. Yankin, V. V. Sizov, O. V. Levin, *ChemElectroChem* **2022**, *9*, DOI 10.1002/celc.202101316.

[37] M. Vilas-Boas, M. J. Henderson, C. Freire, A. R. Hillman, E. Vieil, *Chem. – A Eur. J.*

WILEY-VCH

2000, *6*, 1160.

[38] R. V. Apraksin, Y. A. Volosatova, A. I. Volkov, P. S. Vlasov, D. A. Lukyanov, I. R. Kulikov, S. N. Eliseeva, O. V. Levin, *Electrochim. Acta* **2021**, *368*, 137637.

[39] D. Tomczyk, W. Bukowski, K. Bester, P. Urbaniak, P. Seliger, G. Andrijewski, S. Skrzypek, *New J. Chem.* **2017**, *41*, 2112.

[40] M. V. Novozhilova, E. A. Smirnova, M. P. Karushev, A. M. Timonov, V. V. Malev, O. V. Levin, *Russ. J. Electrochem.* **2016**, *52*, 1183.

[41] E. V. Alekseeva, I. A. Chepurnaya, V. V. Malev, A. M. Timonov, O. V. Levin, *Electrochim. Acta* **2017**, *225*, 378.

[42] M. Nunes, M. Araújo, J. Fonseca, C. Moura, R. Hillman, C. Freire, *ACS Appl. Mater. Interfaces* **2016**, *8*, 14231.

[43] J. Tedim, F. Gonçalves, M. F. R. Pereira, J. L. Figueiredo, C. Moura, C. Freire, A. R. Hillman, *Electrochim. Acta* **2008**, *53*, 6722.

[44] F. Li, Y. Zhang, S. R. Kwon, J. L. Lutkenhaus, *ACS Macro Lett.* **2016**, *5*, 337.

[45] Y. Zhang, J. Li, F. Gao, F. Kang, X. Wang, F. Ye, J. Yang, *Electrochim. Acta* **2012**, *76*, 1.

[46] J. Tedim, A. Carneiro, R. Bessada, S. Patrício, A. L. Magalhães, C. Freire, S. J. Gurman, A. R. Hillman, *J. Electroanal. Chem.* **2007**, *610*, 46.

[47] A. A. Vereshchagin, P. S. Vlasov, A. S. Konev, P. Yang, G. A. Grechishnikova, O. V. Levin, *Electrochim. Acta* **2019**, *295*, 1075.

[48] E. V. Beletskii, Y. A. Volosatova, S. N. Eliseeva, O. V. Levin, *Russ. J. Electrochem.* **2019**, *55*, 339.

[49] K. Łępicka, M. Majewska, R. Nowakowski, W. Kutner, P. Pieta, *Electrochim. Acta* **2019**, *297*, 94.

[50] C. Chen, X. Li, F. Deng, J. Li, *RSC Adv.* **2016**, *6*, 79894.

[51] K. Łępicka, P. Pieta, G. Francius, A. Walcarius, W. Kutner, *Electrochim. Acta* **2019**, *315*, 75.

[52] A. O. Efremova, A. I. Volkov, E. G. Tolstopyatova, V. V. Kondratiev, *J. Alloys Compd.* **2022**, *892*, 162142.

[53] G. Sauerbrey, *Zeitschrift für Phys.* **1959**, *155*, 206.

[54] M. Vilas-Boas, C. Freire, B. de Castro, A. R. Hillman, *J. Phys. Chem. B* **1998**, *102*, 8533.

[55] E. Laviron, *J. Electroanal. Chem. Interfacial Electrochem.* **1979**, *101*, 19.

WILEY-VCH

[56] M. Sterby, R. Emanuelsson, X. Huang, A. Gogoll, M. Strømme, M. Sjödin, *Electrochim. Acta* **2017**, *235*, 356.

[57] E. V. Alekseeva, A. A. Vereshchagin, M. V. Novozhilova, N. A. Panjwani, J. V. Novoselova, D. A. Lukyanov, E. V. Beletskii, J. Behrends, V. V. Sizov, O. V. Levin, *J. Electroanal. Chem.* **2023**, *935*, 117310.

[58] Z. Gao, C. Kvarnström, A. Ivaska, *Electrochim. Acta* **1994**, *39*, 1419.

[59] A. A. Vereschagin, V. V. Sizov, P. S. Vlasov, E. V. Alekseeva, A. S. Konev, O. V. Levin, *New J. Chem.* **2017**, *41*, 13918.

[60] J. Heinze, B. A. Frontana-Uribe, S. Ludwigs, *Chem. Rev.* **2010**, *110*, 4724.

[61] F. Thomas, *Dalt. Trans.* **2016**, *45*, 10866.

[62] O. Rotthaus, O. Jarjayes, F. Thomas, C. Philouze, C. Perez Del Valle, E. Saint-Aman, J. Pierre, *Chem. – A Eur. J.* **2006**, *12*, 2293.

[63] O. Rotthaus, O. Jarjayes, C. Perez Del Valle, C. Philouze, F. Thomas, *Chem. Commun.* **2007**, 4462.

[64] A. Privitera, R. Warren, G. Londi, P. Kaienburg, J. Liu, A. Sperlich, A. E. Lauritzen, O. Thimm, A. Ardavan, D. Beljonne, M. Riede, *J. Mater. Chem. C* **2021**, *9*, 2944.

[65] M. Vilas-Boas, C. Freire, B. de Castro, P. A. Christensen, A. R. Hillman, *Inorg. Chem.* **1997**, *36*, 4919.

[66] S. M. Dale, A. Glidle, A. R. Hillman, *J. Mater. Chem.* **1992**, *2*, 99.

[67] J. Tedim, S. Patrício, J. Fonseca, A. L. Magalhães, C. Moura, A. R. Hillman, C. Freire, *Synth. Met.* **2011**, *161*, 680.

[68] M. Martins, M. V. Boas, B. de Castro, A. R. Hillman, C. Freire, *Electrochim. Acta* **2005**, *51*, 304.

[69] J. Fonseca, J. Tedim, K. Biernacki, A. L. Magalhães, S. J. Gurman, C. Freire, A. R. Hillman, *Electrochim. Acta* **2010**, *55*, 7726.

[70] E. A. Dmitrieva, I. A. Chepurnaya, M. P. Karushev, A. M. Timonov, *Russ. J. Electrochem.* **2019**, *55*, 1039.

[71] J. L. Brédas, J. C. Scott, K. Yakushi, G. B. Street, *Phys. Rev. B* **1984**, *30*, 1023.

[72] K. Łępicka, P. Pieta, A. Shkurenko, P. Borowicz, M. Majewska, M. Rosenkranz, S. Avdoshenko, A. A. Popov, W. Kutner, *J. Phys. Chem. C* **2017**, *121*, 16710.

[73] R. M. Clarke, K. Herasymchuk, T. Storr, *Coord. Chem. Rev.* **2017**, *352*, 67.

[74] E. C. Wu, C. Z. Salamat, O. L. Ruiz, T. Qu, A. Kim, S. H. Tolbert, B. J. Schwartz, *Adv. Funct. Mater.* **2023**, *33*, 19, 2213652.

WILEY-VCH

[75]   C. Song, T. M. Swager, *Org. Lett.* **2008**, *10*, 3575.

[76]   J. Polozhentseva, M. Novozhilova, M. Karushev, *Int. J. Mol. Sci.* **2022**, *23*, 1795.

[77]   J. B. Gerken, S. S. Stahl, *ACS Cent. Sci.* **2015**, *1*, 234.

[78]   E. V. Alekseeva, V. A. Ershov, A. S. Konev, O.V. Levin. *Ecs Transactions.* **2018**, *87*(1), 167.

[79]   L. Bennett, B. Melchers, B. Proppe, **2020**.

SalEn-based redox-conducting polymers are promising materials for energy storage, but their charge transfer mechanism and its effect on electrochemical properties are often poorly understood. This work investigates the effect of geometry modification and introduction of the TEMPO radical into SalEn monomers on the electrochemical properties of respect polymer films and highlights the changes resulting from the unique interactions between polaron-bipolaron particles and redox-active groups, opening up promising applications in batteries and supercapacitors.

A. A. Vereshchagin, A. I. Volkov, J. V. Novoselova, N. A. Panjwani, A. N. Yankin, V. V. Sizov, D. A. Lukyanov, J. Behrends and O. V. Levin*

Harmonizing Energies: The Interplay Between a Nonplanar SalEn-Type Molecule and a TEMPO Moiety in a New Hybrid Energy-Storing Redox-Conducting Polymer